IEEE Access
Multidisciplinary | Rapid Review | Open Access Journal

Received June 10, 2020, accepted June 18, 2020, date of publication June 22, 2020, date of current version July 3, 2020.

Digital Object Identifier 10.1109/ACCESS.2020.3004025

Design and Control of Magnetic Levitation System by Optimizing Fractional Order PID Controller Using Ant Colony Optimization Algorithm

ABDULLAH MUGHEES, (Member, IEEE), AND SYED ALI MOHSIN, (Member, IEEE)
Department of Electrical Engineering, National University of Computer and Emerging Sciences, Islamabad 44000, Pakistan
Corresponding author: Abdullah Mughees (f180867@nu.edu.pk)

ABSTRACT MAGnetic LEVitation (Maglev) is a multi-variable, non-linear and unstable system that is used to levitate a ferromagnetic object in free space. This paper presents the stability control of a levitating object in a magnetic levitation plant using Fractional order PID (FOPID) controller. Fractional calculus, which is used to design the FOPID controller, has been a subject of great interest over the last few decades. FOPID controller has five tunning parameters including two fractional-order parameters (λ and μ). The mathematical model of the Maglev plant is obtained by using first principle modeling and the laboratory model (CE152). Maglev plant and FOPID controller both have been designed in MATLAB-Simulink. The designed model of the Maglev system can be further used in the process of controller design for other applications. The stability of the proposed system is determined via the Routh Hurwitz stability criterion. Ant Colony Optimization (ACO) algorithm and Ziegler Nichols method has been used to fine-tune the parameters of FOPID controller. FOPID controller output results are compared with the traditional IOPID controller for comparative analysis. FOPID controller, due to its extra tuned parameters, has shown extremely efficient results in comparison to the traditional IOPID controller.

INDEX TERMS FOPID controller, fractional calculus, ant colony optimization, Maglev mathematical model, Routh-Hurwitz stability, MATLAB-simulink, first principle modeling.

I. INTRODUCTION

The theory of the magnetic levitation (Maglev) system can be described as the levitation of a ferromagnetic object in free space due to the presence of an electromagnetic field against a gravitational force acting on it. Various modern applications such as magnetic lift, highly efficient platforms, and high velocity magnetic trains use this principle. Removal of heat losses due to the mechanical frictional forces acting on the levitating object is one of the major advantages. This concept is over 100 years old and this idea of frictionless trains was first conceived by American scientists ''Robert Goddard'' and ''Emile Bachelet''. Based on the levitating object's actual and desired position in free space, the amount of current passing through the electromagnetic coil is controlled via the designed controllers to produce the necessary force required to levitate it at the desired position [1].

Earnshaw's theorem proves that stable magnetic levitation can not be achieved using electromagnetic fields that are static. The Maglev system is inherently unstable, non-linear and is influenced by the electromagnetic fluctuations. Closed-loop stability becomes difficult due to these nonlinear electromagnetic forces. Position control of the levitating object becomes quite complex in terms of design due to the constant current passing through the electromagnet [2]. Calculations for levitating object's speed and position can be done to accomplish stable magnetic levitation via a feedback loop that constantly changes the current in one or multiple coils of the electromagnet to modify the motion of the object, thereby creating a mechanism known as servo-mechanism. Attractive and repulsive magnetic levitation systems are the two types that are used to design any system based on Maglev. Figure 1 shows an example of a general attractive Maglev system, where the levitating object is attracted by the electromagnet placed above it against the force of gravity.

The applications of Maglev systems in the field of engineering science can be summarized and categorized as follows [3]:

- aerospace engineering (rocket, spacecraft, etc),

The associate editor coordinating the review of this manuscript and approving it for publication was Feiqi Deng.

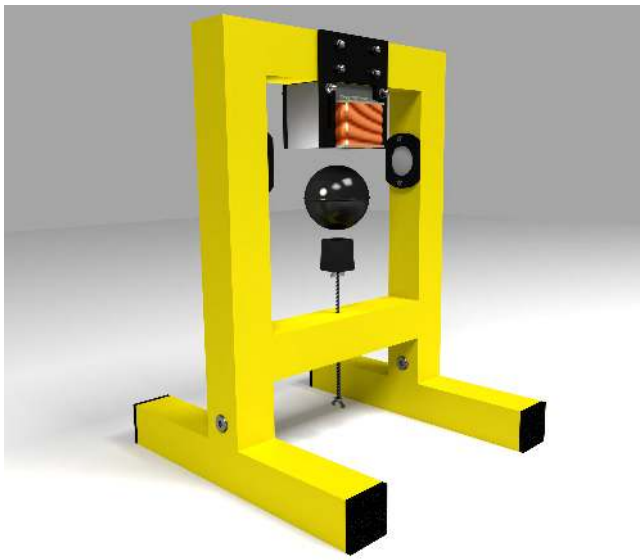

FIGURE 1. Attractive magnetic levitation system.

FIGURE 2. Repulsive magnetic levitation system.

- transportation engineering (personal rapid transit (PRT), Maglev trains, flying cars, etc.),
- military weapons engineering (gun, rocket launchers, etc.),
- environmental engineering (wind turbines for office, home, and industry),
- nuclear engineering (nuclear reactor's centrifuge),
- biomedical engineering (pumping heart, etc.),
- civil engineering (elevators, pump, magnetic bearing, lift, geothermal heat and gas pumps, compressor, fan, chiller, etc.),
- chemical engineering (Beverages and food analyzers, etc.),
- automotive engineering (vehicles, etc.),
- electrical engineering (motors, magnets, levitating objects, etc.),
- advertising engineering (levitation, etc.),
- architectural engineering (bed, lamp, sofa, chair, toy train, etc.),

Due to the vast applications of the Maglev system, the development of a proper control strategy for controlling the system becomes extremely important. Industrial products mostly take advantage of the repulsive magnetic levitation system that is shown in Figure 2.

Maglev system is a fine example of a system that is fundamentally nonlinear and unstable. Designing a device for stable control of Maglev system's is quite difficult due to these properties. The literature review reveals that various control methods are used in designing a controller for the Maglev systems, such as H_∞ control [4], sliding mode control [5], TID and ITD control [6]. Furthermore, neural networks [7], fuzzy logic control [8] and evolutionary algorithms [9] have also been used. A real-time dynamic environment systems are the strong focus of the recent control engineering problems.

A new approach to improve magnetic levitation system performance is reported in [10]. Amplitude from one point in space to another of the levitating object is the controlled parameter during movement. Two position levitation systems with enhanced amplitude efficiency can be achieved using an orthogonal neural network in the traditional levitation control logic [11]–[14]. A self-regressive non-linear orthogonal polynomial network is proposed [15]–[17]. Experiments performed on a system with predefined control signals has shown that the levitation amplitude of the designated levitation object upon surpassing 10^{-4} m doesn't provide sustainable double levitation. The neural network has been developed on the basis of standard sigmoid and tangent functions by utilizing the real observational evidence [18]–[22]. Default activation functions were replaced with new orthogonal polynomial functions [23]–[25]. Stable levitation for two position system is achieved after parameter optimization at an amplitude of 10^{-3}. The results concluded that the performance of amplitude is improved through a non-linear autoregressive neural network with a simple control logic and appropriate activation function.

The design of a robust PID-type magnetic levitation system (Fuzzy-PID) to improve system dynamics and stability is reported in [26]. A proposed objective function optimized the controller parameters with response characteristics in time domain using Cuckoo Search (CS) algorithm [27]–[29]. The implementation of the developed controller is assessed by simulation experiments for varying environments, like load interference and reference changes [30], [31]. The comparison of Cuckoo Search algorithm based FOPID and PID is included. The yielded results suggest that the Fuzzy-PID based on CS performs better when it comes to steady state error, settling time, and overshoot. The comparison indicates that the Fuzzy - PID controller based on Cuckoo search algorithm surpasses the performance of conventional FOPID and PID controller and also it has less control effort.

A study on magnetic levitation system model and control has been presented in [32]. The model considers the ball's

angular position, and the electromagnetic (EM) parameters are approximated by neural networks [33], [34]. A combination of neural network and non-linear system yields a neural network controller, and the Lyapunov approach ensures its stability [35]. A multi-stage controller is compared for trajectory tracking with the proposed controller in the maglev system.

To control the position in a maglev system, a super twisting control (STC) based robust high-order sliding mode control method is proposed in [36]. The homogeneity principle is utilized to modify the sliding surface [37]. Effective disturbance rejection, finite time reachability, and continuous control without chattering can be successfully achieved via the proposed controller [38], [39]. Lyapunov stability theorem is used to analyse the settling time estimation and the closed loop stability of the system [40]–[43].

There are many applications where magnetic levitation systems are of paramount importance. Development of robust tracking and high-performance control system becomes challenging for the researchers due to their non-linearity and high instability. Therefore, in [44] systems with uncertain structure and parameters (uncertain inputs with non-linearity) have been improved via an adaptive fuzzy backstepping control and this improvement is then applied to a maglev system. Uncertain maglev inputs with non-linearity, partially known inputs, and unknown inputs are estimated via an adaptive fuzzy system. Based on Lyapunov analysis, an adaptation law is obtained for better performance tracking and stability of a closed loop system. Symbiotic Organism Search optimization algorithm initialized adaptive and control parameters due to magnetic levitation system instability and strong non - linearity. A laboratory experimental system simulation research and implementation has validated the proposed control methodology.

To compensate the non-linear dynamics of system, a nonlinear controller has been designed in [45]. Control input is applied in the proposed method for the generation of the required flux in the system. The object is suspended in free space, by utilizing this generated magnetic flux, at a specific distance from the electromagnetic coil [46]–[48]. The magnetic force accelerates the levitating object at a precise level to cancel the effect of gravitational force acting on it, in order for the levitation to occur [49]–[52]. The asymptotic stability of the system is checked via Lyapunov theory for every non-linear controller [18], [53], [54]. The proposed controller is analysed and evaluated after the simulations in MATLAB / Simulink. In addition, a comparison between the proposed controller and a linear (PI) controller is conducted and results are discussed.

The designing and implementation of a Model Predictive Control (MPC)-based reference governor on an industrial-like microcontroller is reported in [55]. The optimum set-points are achieved by utilizing the governor's task for the Proportional-Summation-Difference (PSD) controller [56]–[59]. Off-line synthesizes the Model Predictive Control (MPC) based governor as a Piecewise Affine (PWA) function that maps measurements to optimal references [60]–[62]. Binary search tree is used for encoding of the PWA function for a memory-efficient and quick implementation. Because of this any conventional hardware can enable the governor to operate at a scale of sub-milliseconds. The maglev system in laboratory is used to validate the proposed methodology [63]. The PSD controller controls the coordinates, in the magnetic field, of the levitating object in free space.

A nonlinear optimal controller is designed in [64], using stable multiple theories, based on the theory developed in order to study the constraints and their classes in the system [65]. One feature of this method is the need to solve a discontinuous ''Hamiltonian syste'' [66]. The solutions of Hamiltonian system are demonstrated by the discussion in this research of stable controller design for the complex systems [67]. The yielded results demonstrate that the system can better deal with acceleration constraints by using the non-linear controller. Similarly, a maglev control system has been designed in [68]. The complex and nonlinear model of the system around the operating point is linearized. Through a linear system, internal current and multiple control loops along with an external position loop have been designed. The proposed methodology and dynamic response of the system is verified via experimental results and simulations.

Design of a controller that can handle the complexity of the non-linearities in an unstable system is one most difficult task for the researchers. Many forms of work have already been carried out in this area so far and many are still in the process of reducing the control effort by designing the most efficient control designs. Control researchers have successfully developed and implemented various control methods, such as ''Proportional Integral Derivative (PID) control'' ''Proportional Integral (PI) control'', ''Proportional Derivative (PD) control'', etc. Between the various combinations of the controller, the PID controller is the most consistently used controller by the control engineers for a long time due to its ease of implementation, performance delivery capability and simple structure. Regarding the benefits of ensuring good robustness with adequate performance, there is still a chance of achieving more efficient results by changing the original design of the conventional PID controller [69]. The adjustment can change the current control structure from 1 degree of freedom (DOF) or 2 DOF [70], to fractional order instead of the conventional integer order.

Traditional controllers such as PID are not able to perfectly handle the non-linearity of an unstable system. To control the magnetic levitation system (MLS), conventional controllers like Fuzzy, PID, PI controller and other controllers are being widely used [71]. Here, MLS is controlled using the FOPID controller that is a control technique considered as non-conventional. The idea of fractional calculus is used in this technique to achieve higher accuracy and precision in results. Over the last few decades, the most considerable concern has been given to the fractional calculus. There are areas that

have chaotic and viscoelastic systems with fractional calculus equations representing their dynamics [72].

FOPID controller provides better control because of two extra tuning parameters (λ and μ), fast response towards reference signal, more flexibility, higher stability and better handling of a non-linear systems [73]. Maglev systems are non-linear and the PID controller is not suited for nonlinear systems [74]. Therefore, FOPID is used to control the position and settling time of an object in the magnetic field. It aims to increase the stability and efficiency of the system by decreasing the settling time.

Instability and nonlinearity of the open-loop are two aspects of a MLS that are represented by an extremely nonlinear differential equation [75]. This has resulted in feedback control being used for system stability. Therefore, feedback is controlled using various controllers and most commonly PID controller to stabilize the system. Various controllers and algorithms have been used for controlling the Maglev system in the literature. In [76], developments of FOPID controllers have been highlighted, along with their tuning method. Often discussed are software tools related to the design of FOPID controllers.

Using the firefly algorithm, FOPID can be used to power the Maglev system. The PID and FOPID controller parameters are adjusted by the Firefly Algorithm (FA). This meta-heuristic algorithm is dependent on the motion of the fireflies to produce an extremely desirable and safer path. Using control toolbox and fractional-order modeling, FOPID and PID controllers have been implemented in MATLAB and SIMULINK. Results in real-time indicated adequate steady-state and transient responses to controllers. The FOPID controller turned out to be much more efficient than the PID [77].

Particle swarm optimization (PSO) algorithm, genetic search algorithm (GSA), and their hybrid PSOGSA have been used to control the Maglev system using the FOPID controller. The results of the experiment retrieved from a broad range of test signals indicate that the PSOGSA hybrid algorithm is more effective with sufficiently stable and transient responses than the individual equivalents of itself [78]. A sliding mode controller (SMC) has been used to control the magnetic levitation system. The proposed sliding mode controller shows that the system has a high degree of rigidity and a more widespread and effective bending of suppressing disturbance relative to a traditional PID controller control strategy [79].

The FOPID controller has been used to control the Maglev system using a genetic algorithm. FOPID controller has control constraints that have been adapted from the performance analysis and the methodology of genetic algorithm optimization. It is noted that the FOPID controller can efficiently manage the plant with a small error of 13.04 % in real-time mode and 5.66 % in simulation mode. It is also reported that the actual and desired ball position in the case of FOPID is very close as compare to other integer order PD and PID controllers [80].

FOPID controller that uses a combination of the Genetic Search Algorithm and Particle Swarm Optimization (PSOGSA), to make a new hybrid algorithm, has been proposed. This research aimed at stabilizing a levitating ferromagnetic object in the magnetic levitation system, as well as regulating its location to track a single reference. FOPID performance turned out to be much more efficient than that of the traditional PID controller [78].

A Fuzzy PID controller has been designed in [81], where an improved Fuzzy Adaptive PID controller (IFPID) has been reported. The algorithm is theoretically designed by nonlinear fuzzy mapping. Results show that higher anti-interference ability, adaptability to changing parameters, better dynamic property and stability is achieved using the IFPID controller. Neural Network PID control method has also been implemented for control of the Maglev system. K_p and K_D parameters are adjusted using the neural network, while K_I is not treated. These results showed even better adaptability and robustness and higher efficiency for the system [82].

PID controller with a variable fuzzy technique is introduced in [83]. The variable universe method is used along with the theory of the variable universe fuzzy PID algorithm. Results showed improved control accuracy, dynamic and static performance. There are various nature-inspired intelligent optimizing algorithms that have been used in the past for controlling the Maglev system. A particle swarm optimization (PSO) algorithm has been used with a PID controller to control the Maglev system. The reliability of the experimental PID-PSO control system has been confirmed using experimental results and numerical simulations. Results indicate desirable system efficiency in control and robustness to uncertainties [84].

Gravitational search algorithm (GSA) has been introduced in [74], along with its hybrid model with PSA. Research carried out using GSA, PSA and hybrid of both GSAPSA. Results indicate that the GSAPSA hybrid algorithm is more efficient than the individual equivalents of itself, with adequate steady-state and transient responses. The firefly algorithm is used to optimize several controller parameters for the Maglev device. Firefly algorithm controls PID and FOPID controller parameters. FOPID controller has much better performance than PID [77].

Teaching learning based optimization (TLBO) algorithm has been reported in [85]. TLBO's search algorithm has two stages, the process of instructor and learner. The implemented performance index is defined by the integral time square error (ITSE). Comparing this new technique with traditional control techniques concludes the corroboration of the new technique. The methodology proposed yielded results that were more effective than traditional techniques. Big-Bang Big-crunch (BBBC) and its hybrid model with the Genetic Algorithm (GA) have been used with the FOPID controller for controlling the Maglev system. Results show that the performance of the BBBC based FOPID controller is higher than that of the GA-optimized FOPID controller [86].

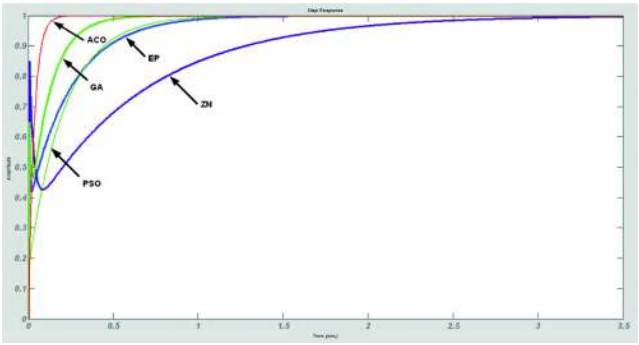

FIGURE 3. Comparison of various algorithms with the traditional PID controller [89].

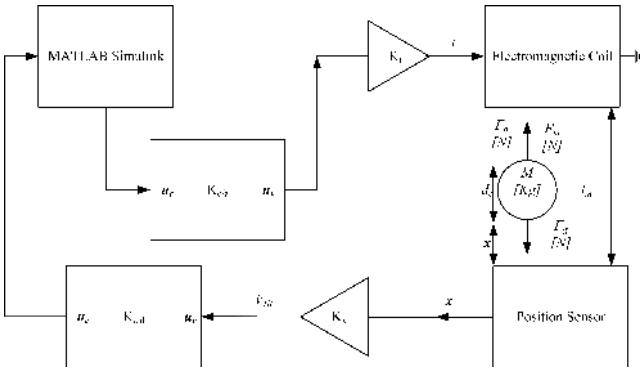

FIGURE 4. Mathematical modeling structure for Maglev system.

In [87], one of the most advanced and efficient Bacteria Foraging algorithm is introduced for a Maglev system. MATLAB system identification toolbox is used for system validation with output resulting in the best fit of 99.83 %. The optimization of the conventional PID controller is stronger than the built-in PID controller. PSA with a weight of mixed inertia has been used in [88]. Results of the simulation show that the robustness and control efficiency of the PSA-PID based mixed inertia weight is significantly lower than that of the 3-PSA-PID controllers based on individual inertia weights.

Even though many algorithms in the literature have shown efficient results but there are limitations that require further improvements. In the PSA-GA hybrid model, there is a need to consider a statistically convergent approach through multiple simulations. Being a stochastic algorithm, it may have to face challenges for complying with the constraints of equality. Convergence speed slows down in GSA at a relatively late search stage. Falling into an optimum local solution becomes quite easy for almost all the algorithms mentioned above. The firefly algorithm has a high chance of being stuck in optimum local solution and sluggish converging speed.

In this research Ant Colony Optimization (ACO) algorithm is used, to optimize the tuning parameters of FOPID controller, which has positive feedback mechanism, a discrete optimization technique, strong robustness, high reliability, fast convergence, high flexibility, fewer setting parameters, stability to explore local solutions, ease of implementation, the capability of combining with other algorithms and ability to handle the objective cost. Figure 3 shows that with the traditional PID controller, ACO is the most efficient algorithm as compared to various other algorithms. Ziegler Nicholas's method has also been used to optimize the parameters of FOPID controller for comparative analysis.

This paper is organized in the following order. Section II explains the mathematical model of the magnetic levitation system designed in MATLAB-Simulink. Section III analyzes the stability of the designed system. The results of the proposed methodology are shown in Section IV. Section VII provides a comparative analysis of the proposed system. Finally, Section VIII concludes the paper with conclusions and future work.

II. MATHEMATICAL MODEL OF MAGLEV SYSTEM IN SIMULINK MATLAB

Mathematical modeling of the Maglev system can be used to investigate the behavior and properties of the modeled plants without actually testing on the real Maglev system. Hence, damage risk and technological faults on the real Maglev system during the test are avoided. There are two methods to model the Maglev system plant; the black box method and the white box method (first principle modeling). Such approaches provide the plant's physical and mathematical analysis.

The black box method is used for specific Maglev system plants. It is focused on the evaluation of the Maglev system's input-output signals [90]. No information is required about the physical theory of the plant being controlled and the model obtained is valid only for the signals that were used for its calculation. The first principle modeling or white box method gives the traditional model of the plant, which is valid with a wide range of plant states and inputs. Physical laws and analysis of the modeled plant are combined to create the white box [91]. For plants with few parameters, first principle modeling is suitable. This is useful in getting the basic data of the plant being controlled.

This research utilizes the first principle modeling for deriving the basic relations and the plant model is further enhanced by taking a few measurements into account. This technique is known as the grey box method [92]. The goal is to create and develop the Maglev system's mathematical model in SIMULINK-MATLAB. Figure 4 describes the core construction of the mathematical model for the Maglev system.

Maglev system is an unstable and nonlinear dynamic system with a single output and input [93]. The output signal contains the information on the location of the levitating object and the input signal is the control signal [94]. The values of both signals are scaled according to the required range of the plant unit (PU).

A. ARCHITECTURE OF THE MAGLEV SYSTEM

The Maglev system consists of an electromagnet, power source, IR sensors for measuring the position of the levitating object, D/A and A/D converters, A/D outputs and inputs,

timers, counters, electronic drivers and a controller for the processing of all the data. The modeled Maglev system can be divided into the following parts;

- D/A and A/D converters.
- IR position sensor
- Electronic amplifier
- Levitating object and electromagnet coil

The electromagnetic force due to the presence of the magnetic field of an electromagnet, which is created by the energy source through an electronic amplifier connected to the Digital/Analog converter, levitates the ferromagnetic object in the air. IR position sensor represented by the inductive linear sensor that is connected to the Analog/Digital converter is used for measuring the position of the levitating object. SIMULINK-MATLAB is used as a transceiver for measured and control parameters both.

B. WORKING PRINCIPLE OF THE SYSTEM

Maglev is an unstable nonlinear dynamic system with a single output and input. When a specific threshold is crossed, an input control signal is fed to the electromagnet through the system. This results in an increased force of attraction between the levitating object and the electromagnet, which causes the levitating object to move upwards and accelerate until it stops upon hitting the core of the electromagnet. This phenomenon occurs when the electromagnetic force from the electromagnet overcomes the gravity force acting on the levitating object. During the period of motion, the acceleration of the levitating object grows as a function of the magnetic field acting on the object that becomes stronger as it moves near to the magnetic core. This accelerating force and the levitating object both stop when the object hits the obstacle (physical structure of electromagnet).

An increase at the input signal causes an increase in the electromagnetic force that results in rapid growth in the accelerating force of the object. If the input signal value falls below the lower threshold value, the levitating object falls. As now, the electromagnetic force does not overcome the gravitational force acting on the levitating object. Step signal is used for the tested input signal as other signals (e.g. sinus or ramp signal) do not provide suitable information for the value. Once the electromagnetic force of the electromagnet is strong enough, it attracts the levitating object towards its core, even with the increasing input signal.

C. DIGITAL-ANALOG CONVERTERS (D/A AND A/D)

The purpose of digital/analog converter is to change the digital-signal coming from the controller U_c into a voltage signal that is analog in nature U_v, which is then fed to the electromagnetic coil. This digital/analog conversion is described by the linear (1):

$$U_v = K_{d/a} \cdot U_c \tag{1}$$

where U_v is defined as the input voltage signal to the electromagnet's coil or the digital/analog converter output. U_c is the input signal to the digital/analog converter from the controller and $K_{d/a}$ is the gain of digital/analog converter.

The digital/analog converter maps the input signal $-1< U_c <1$ to the range $0< U_v <5$. As the Maglev system is constructed for this range. Therefore, the input signal must be constrained and mapped to the desired values. This makes the digital/analog converter gain $K_{d/a}$ of 10 V/PU. Similarly, analog/digital converters are used to convert back the analog U_v signal to its digital form U_c. This is represented using the linear relationship shown in (2):

$$U_c = K_{a/d} \cdot U_v \tag{2}$$

The analog/digital converter maps the input signal $0< U_v <5$ to the range $-1< U_c <1$. This makes the analog/digital converter gain$K_{a/d}$ of 0.1 PU/V.

TABLE 1. Boundary values for calculating the gain of IR position sensor.

x_i(m)	u_{ci} (V)	V_{IR_i}(V)
0	0.00354	0.03537
0.0057	0.48384	4.83840

D. IR POSITION SENSOR

The position (x) of the levitating object is measured using the inductive IR position sensor. The maximum height declared (l_m) is considered as the difference between the bottom end of the electromagnetic coil and the IR position sensor (l_i). The diameter of the levitating object is d_0. The analog / digital converter reading is used to measure the location of the levitating object in space. Sensor voltage varies according to the direction of the levitating object. The relation between the voltage signal of the levitating object and its location is defined by (3):

$$U_c = K_{a/d} \cdot U_v \tag{3}$$

Voltage of position sensor can be determined by (4):

$$V_{IR} = K_x * x + V_0 \tag{4}$$

where V_{IR} is the voltage (V) of the IR position sensor, V_0 is the offset voltage (V) of position sensor, (x) defines the location of the levitating object in space and (K_x) is defined as the gain of IR position sensor (V/m).

Using experimental results, calibration has to be done. Firstly, distance travel or maximum height declared (l_m) will be calculated by taking the difference between the bottom end of the electromagnetic coil and the IR position sensor ($l_i = 18.4 * 10^{-3}m$) and the diameter of the levitating object ($d_o = 12.7 * 10^{-3}m$).

$$l_m = l_i - d_o = 5.7 * 10^{-3}m$$

The boundary values have been noted in Table 1 to calculate the gain of the IR position sensor.

Considering the input signal as zero, initial value from the IR position sensor is taken that is the offset of position sensor:

$$U_o = U_1 = 0.03537V$$
$$K_x = \frac{y_2 - y_1}{x_2 - x_1} = 826.8525V/m$$

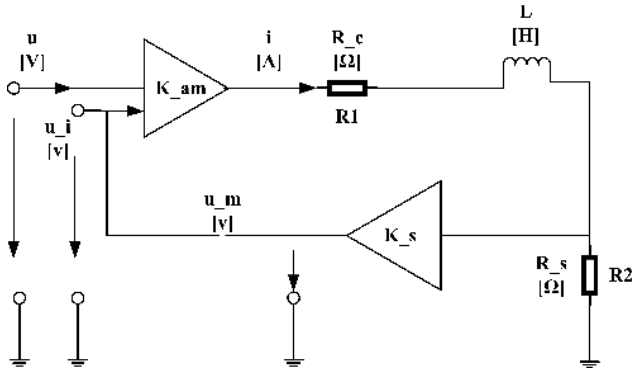

FIGURE 5. Power amplifier internal structure.

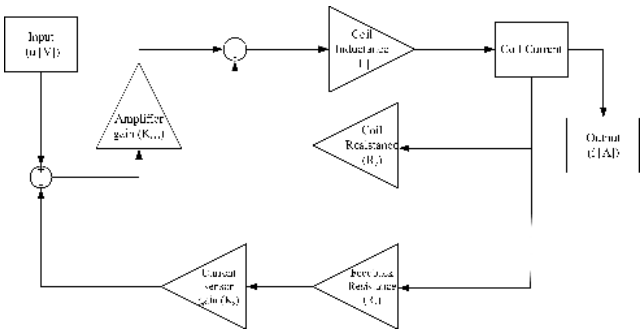

FIGURE 6. Block diagram of simulated power amplifier.

E. ELECTRONIC AMPLIFIER

Output current is fed into the electromagnetic coil through the power amplifier that acts as a transconductance amplifier. This output current is produced from power amplifier through the differential voltage between the ($u = u_c$) and ($u_i = u_{ci}$), from the digital/analog converter. This electronic power amplifier acts as a current stabilizer and constant instantaneous current source. The internal structure of this power amplifier is shown in Figure 5. where K_{am} stands for amplifier gain [-], K_s stands for current sensor gain [-], L represents inductance of the coil [H], R_s is resistance of feedback resistor [Ω] and R_c is the resistance of the coil [Ω]. (5) and (6) are used to represent the power amplifier and (7) is obtained by considering zero initial conditions and taking Laplace transform.

$$u_m = \frac{d_i}{d_t}L + i(R_c + R_s) \tag{5}$$

$$u_m = K_{am}(u - R_s K_s i) \tag{6}$$

$$\frac{I_s}{U_s} = \frac{\frac{K_{am}}{R_c+R_s+K_{am}R_s k_s}}{\frac{KL}{R_c+R_s+K_{am}K_s K_s)S} + 1} \tag{7}$$

Simulated structure of the power amplifier is represented in Figure 6. The first order transfer function can be used to simplify (7) in order to yield (8).

$$G_{PA}(s) = \frac{I(s)}{U(s)} = \frac{K_i(s)}{T_a(s) + 1} \tag{8}$$

where time constant of amplifier is defined by T_a and gain of amplifier is K_i. Typical parameters for each element of the power amplifier and coil (Humusoft manual) are; $K_{am} = 100.000, K_s = 13.333, L = 30.011 * 10^3, R_c = 3.500\Omega, R_s = 25.133 * 10^{-2}\Omega$. Putting these values in (7) to calculate the values of time constant and gain of power amplifier:

$$T_a = 8.902^{-5}s$$
$$K_i = 0.297A/V$$

It can be observed from the yielded results that the time constant T_a is quite small and can be neglected before proceeding further. Therefore, the gain of the amplifier is taken into account only.

F. LEVITATING OBJECT AND ELECTROMAGNET COIL

A method that is known as ''Lagrange's method'' has been used to model the levitating object and the electromagnet coil. Equations of motion are dependent on all the balancing forces acting on the levitating object. (9) represents the force of acceleration acting on the levitating object.

$$F_a = F_{em} - F_g \tag{9}$$

where F_a is the acceleration force acting on the levitating object (N), F_{em} is the electromagnetic force generated by the coil (N) and F_g is the gravitation force acting on the levitating object (N).

The constant gravitational force (F_g) is dependent on the mass of the levitating object. It works against the direction of the electromagnetic force (F_{em}) generated by passing an electric current through the coil. It can be seen that the lift force on the levitating object will only exist when the acceleration force (F_a) is greater than zero (e.g. electromagnetic force created by the coil is greater than the gravitational force acting on the levitating object).

Second-order non-linear differential equations can be found in (10). The output variable can be defined as the location of the levitating object in space and input variable as an electric current passing through the electromagnetic coil.

$$m_k \frac{dx^2}{d^2t} + K_{fv}\frac{dx}{dt} = \frac{i^2 K_c}{x - x_o} - m_k g \tag{10}$$

where,

x = location of the levitating object (m),
m_k = mass of the levitating object (kg),
g = acceleration of gravity (ms^{-2}),
K_{fv} = dumping constant ($Nms^{-}1$),
K_c = constant for coil,
X_o = offset of the coil (m),
i = current passing through the coil (A).

It can be seen that the electromagnetic force acting on the levitating body is defined by two parameters (current and position). Furthermore, the consideration of damping force acting on the levitating object is also taken into account. Mass

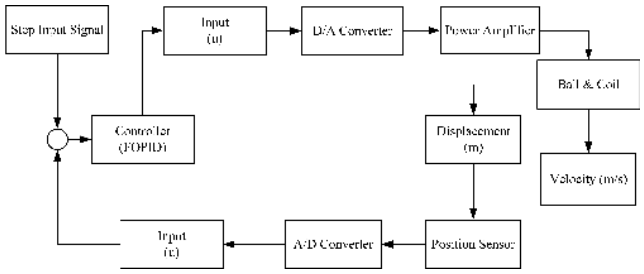

FIGURE 7. Maglev interconnections model.

of the levitating object can be calculated using the numerical values of its parameters. The mass of an object with density $\rho = 7800\ \text{kgm}^{-3}$ and diameter $d_o = 12.7 \times 10^{-3} m$ is calculated in (11):

$$m_k = \rho V_k = \rho \frac{4}{3}\pi(\frac{d_k}{2})^3 = 8.37 \times 10^{-3} kg \tag{11}$$

The value of the damping constant K_{fv} has been used from the literature, where it has been found using the trial-and-error method through comparison of real experimental data. As its value cannot be measured by a direct or any dedicated experiment.

$$K_{fv} = 0.0195(Nsm^{-1})$$

The Maglev signal processing model is represented by the block in Figure 7:

A single input single output non-linear dynamic Maglev system has been designed in SIMULINK-MATLAB. The power amplifier is fed with an input voltage signal through D/A converter, which produces an output current that passes through the coil, resulting in the creation of the magnetic field that lifts the levitating object in free space. The IR position sensor measures the location of the levitating object in free space. The coil and power amplifier models are used to represent the magnetic field produced by the electromagnetic coil. The output is a current signal that is the input to the electromagnetic inductive coil and feed-back is a voltage signal. Variations in the dynamics and non-linearities caused by saturated coil have been modeled. IOPID controller is used to implementing a previous technique and perform comparative analysis with the FOPID controller.

III. STABILITY ANALYSIS OF MAGNETIC LEVITATION SYSTEM

There are three major parameters that are considered for the design of any control system; steady-state errors, transient response, and stability. If a system is not stable, steady-state errors and transient response are moot points. Hence, stability is considered as the most important parameter for the design of any control system.

Linear time-invariant (LTI) system is considered stable if the transient response approaches zero as time goes to infinity. If the transient response approaches infinity with time, the system is labeled as unstable. There is a third stage known as marginal stability that is when the transient response of the system neither grows nor decays as time goes to infinity. The total response of a system is defined as the sum of transient response (tr) and steady-state response (ssr), as shown in (12).

$$c_{total}(t) = c_{tr}(t) + c_{ssr}(t) \tag{12}$$

Bounded Input Bounded Output (BIBO) stability is used to define the stability of the system by using the total response of the system instead of transient response. The system is marked stable when all bounded inputs (BI) yield bounded outputs (BO) and it is marked unstable if any of the bounded input gives an output that is unbounded. Practically any unstable system that has a transient or zero-input response which increases with time can be considered as harmful to human life, systems or adjacent property. In a time-response plot of a practical system, instability occurs when the transient response grows without any bound and causes the total response to never reach a steady state.

The roots or poles can be used to define the stability of a closed-loop system. Poles in the left half-plane (LHP) of s-plane will have a negative real part and the result will be a damped sinusoidal or pure exponential decay of transient response. Poles in the right half-plane (RHP) will have a positive real part and the result will be a pure exponentially increasing sinusoidal transient response. Therefore, the system is stable if the poles of the transfer function of a closed-loop system lie in the left half-plane.

A marginally stable system will have the imaginary axis poles of multiplicity '1' that neither decays or increases in amplitude and will result in pure sinusoidal oscillations as the transient response. Thus, the system is marginally stable if the poles are in the left half-plane and the transfer function of the closed-loop system only has imaginary axis poles of multiplicity 1.

The mathematical model of the Maglev system has been represented in the previous section. The Laplace transformation of this model has been analyzed and the block diagram of the Maglev system with its components is shown in Figure 8.

A single transfer function has been achieved by reducing the multiple subsystems to convert the closed-loop system to an open-loop transfer function. (13) shows the equivalent open-loop transfer function model that has been obtained by using the reduction of multiple subsystem method.

$$T \cdot F_{Maglev} = \frac{a}{b} \tag{13}$$

where

$$a = 4.43(2s+1)(3s+1000)^4,$$
$$b = 6.003s^6 + 8.02e3s^5 + 4.025e6s^4 + 9.009e8s^3 + 7.67e10s^2 + 2.152e11s + 8.854e10.$$

The transfer function for the FOPID controller has also been evaluated for stability analysis. A step input to FOPID controller yield 24 state variables. The response of the FOPID controller with a step input is shown in Figure 9.

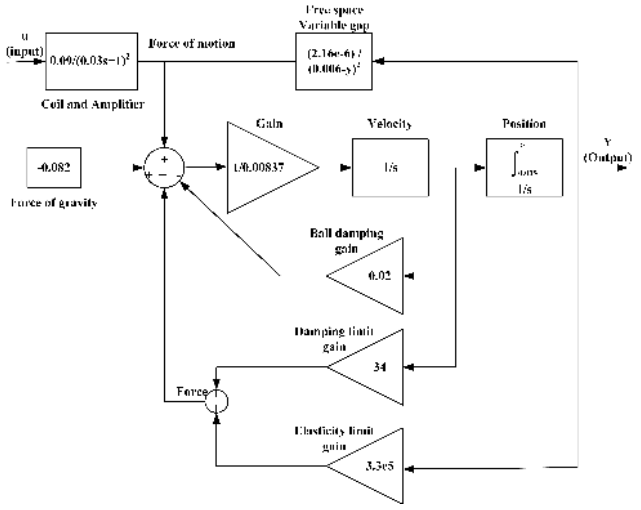

FIGURE 8. Block diagram of Maglev system's internal structure.

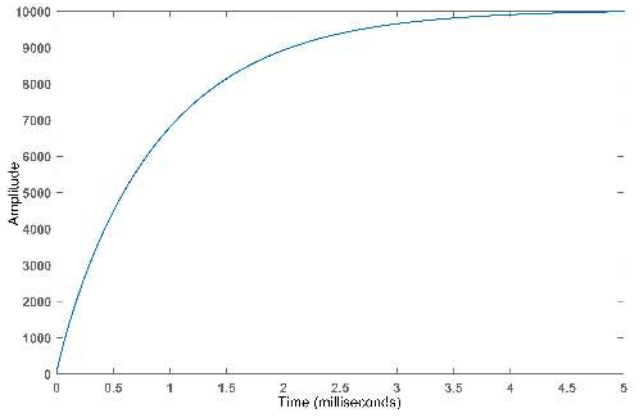

FIGURE 9. Step response of FOPID controller.

(14) shows the transfer function for the FOPID controller. Stability analysis using Routh Hurwitz Criterion has been performed on both the FOPID controller and the Maglev system.

$$T.F_{FOPID} = \frac{c}{d} \tag{14}$$

$c = 0.5\,s^{24} + 1.274e05\,s^{23} + 2.417e08\,s^{22} + 1.523e11\,s^{21} + 4.314e13\,s^{20} + 5.984e15\,s^{19} + 4.293e17\,s^{18} + 1.625e19\,s^{17} + 3.342e20\,s^{16} + 3.832e21\,s^{15} + 2.582e22\,s^{14} + 1.081e23\,s^{13} + 2.937e23\,s^{12} + 5.073e23\,s^{11} + 5.295e23\,s^{10} + 3.15e23\,s^{9} + 1.03e23\,s^{8} + 1.84e22\,s^{7} + 1.77e21\,s^{6} + 8.96e19\,s^{5} + 2.39e18\,s^{4} + 3.2700e16\,s^{3} + 2.2220e14\,s^{2} + 6.8130e11\,s + 7.5410e08,$

$d = s^{24} + 3685\,s^{23} + 5.308e06\,s^{22} + 3.797e09\,s^{21} + 1.435e12\,s^{20} + 2.924e14\,s^{19} + 3.198e16\,s^{18} + 1.882e19\,s^{17} + 5.918e19\,s^{16} + 9.975e20\,s^{15} + 8.96e21\,s^{14} + 4.308e22\,s^{13} + 1.103e23\,s^{12} + 1.511e23\,s^{11} + 1.101e23\,s^{10} + 4.288e22\,s^{9} + 8.877e21\,s^{8} + 9.799e20\,s^{7} + 5.722e19\,s^{6} + 1.767e18\,s^{5} + 2.839e16\,s^{4} + 2.3380e16\,s^{3} + 9.3910e14\,s^{2} + 1.685e09\,s + 1.000e06.$

TABLE 2. Routh table for (15).

s^n	a_n	a_{n-2}	a_{n-4}
s^4	a_4	a_2	a_0
s^3	a_3	a_1	0
s^2	$-\frac{\begin{vmatrix} a_4 & a_2 \\ a_3 & a_1 \end{vmatrix}}{a_3} = b_1$	$-\frac{\begin{vmatrix} a_4 & a_o \\ a_3 & 0 \end{vmatrix}}{a_3} = b_2$	$-\frac{\begin{vmatrix} a_4 & 0 \\ a_3 & 0 \end{vmatrix}}{a_3} = 0$
s^1	$-\frac{\begin{vmatrix} a_3 & a_1 \\ b_1 & b_2 \end{vmatrix}}{b_1} = c_1$	$-\frac{\begin{vmatrix} a_3 & 0 \\ b_1 & 0 \end{vmatrix}}{b_1} = 0$	$-\frac{\begin{vmatrix} a_3 & 0 \\ b_1 & 0 \end{vmatrix}}{b_1} = 0$
s^0	$-\frac{\begin{vmatrix} b_1 & b_2 \\ c_1 & 0 \end{vmatrix}}{c_1} = d_1$	$-\frac{\begin{vmatrix} b_1 & 0 \\ c_1 & 0 \end{vmatrix}}{c_1} = 0$	$-\frac{\begin{vmatrix} b_1 & 0 \\ c_1 & 0 \end{vmatrix}}{c_1} = 0$

ROUTH HURWITZ CRITERION

It is a method that can evaluate the stability of a system without the need to find the actual poles of the system. This method allows determining the number of poles in the LHP, RHP or imaginary ($j\omega$) axis, rather than finding the exact coordinates of the poles. Hence, in each section of the s-plane, Routh Hurwitz Criterion only enables us to determine the number of roots or poles. The method can be divided into two steps:

1) Routh Table: A data table based on the coefficients of the s in the denominator of a given transfer function. (15) describes a general transfer function. The table is initiated by marking the rows with powers of s from the highest (s^4) to lowest power (s^0) of the denominator of the transfer function given in (15). The next row is filled by starting with the coefficient (a_4) of the highest power (s^4) in the denominator of the transfer function and list every other coefficient, skipping the coefficient of consecutive power of s, horizontally in the first row. Now, the second row is filled horizontally by starting with the next highest power (s^3) coefficient (a_3) and listing all the skipped coefficients of the first row.
The remaining rows are filled by entering the negative determinant of the items listed in the two rows directly above the item being calculated, divided by the first coefficient listed in the column that is directly above it. The yielded Routh table for the transfer function of (15) is shown in Table 2

$$T \cdot S_{General} = \frac{C_{(s)}}{a_4 s^4 + a_3 s^3 + a_2 s^2 + a_1 s + a_0} \tag{15}$$

2) Routh Table Interpretation: The data entered in the Routh table must be interpreted to determine the number of poles in LHP, RHP or imaginary ($j\omega$) axis. This method is of paramount importance for determining the stability of the system when an unknown variable is present in the denominator of the transfer function for the system.
As system stability is to be analyzed, poles of the system in the denominator of the transfer function are the focus of our attention. Routh table is applied to the systems that have poles in the left or right half planes only. We find an entire row of zeros in the Routh table if the system has imaginary ($j\omega$) roots. Routh Hurwitz

TABLE 3. Routh table for Maglev system.

s^n	a^n	a^{n-2}	a^{n-4}	a^{n-6}
s^6	0.0000	0.0000	0.7669	0.8854
s^5	0.0000	0.0090	2.1521	0
s^4	0.0000	0.7653	0.8854	0
s^3	0.0072	2.1499	0	0
s^2	0.7552	0.8854	0	0
s^1	2.1415	0	0	0
s^0	0.8854	0	0	0

criterion simply states that "*the number of roots of the polynomial that are in the right half-plane is equal to the number of sign changes in the first column of Routh table*".

There are two special cases that can occur in a Routh table:

a) Routh table with Zero in the first column:
If zero is the first entity in any row of the Routh table, forming the next row will require division by zero. Hence, zero can be replaced by an epsilon (ϵ) symbol for the calculations of the next row elements to complete the Routh table. The sign of epsilon ϵ symbol can be taken as either positive or negative, results will always be the same.

b) Entire row of zeros in the Routh table:
In this case, the row directly above the row of zeros is utilized by considering its coefficients as elements for the row of zeros to form an auxiliary polynomial. Then we differentiate this auxiliary polynomial with respect to s and the row of zeros is replaced with the yielded coefficients with respective powers of s.
The polynomials responsible for creating the entire row of zeros are pure even factors of the original polynomial with symmetric poles about the origin. In the Routh table, these even polynomials are always found in the previous row to the row with only zero entities. Symmetrical poles of these even polynomials yield the same number of poles in LHP as in RHP. The remaining poles, if any, must be on the imaginary ($j\omega$) axis.

As any system can be declared as a stable system, If it has all its poles or roots in the left-half of s-plane. Therefore, for a stable system, there will be no sign changes in the coefficients of the entities in the first column of the Routh table. Routh Table for both FOPID and Maglev system are generated using MATLAB. The Routh table obtained for the Maglev system is shown in Table 3.

It can be observed that there are no sign changes in the first column of the yielded Routh table as well. The designed Maglev system is stable. Although, only the existence of poles in the left half-plane of s plane is determined up to this point. The roots of Maglev's open-loop transfer function are determined to locate the exact position of all the poles in the s plane. The poles calculated for the Maglev system are:

$$\begin{aligned} &POLES_{MAGLEV} \\ &= -2.389481 - 0.500000 - 340.887793 \\ &\quad - 7.464606i - 340.887793 \\ &\quad + 7.464606i - 325.778730 - 7.637230i - 325.778730 \\ &\quad - 7.637230i \end{aligned}$$

Similarly, the Routh table for the FOPID controller is generated and the results are shown in Table 4.

It can be observed that entities in the first column of the yielded Routh table for FOPID controller have no sign changes. Hence, it can be concluded that the designed FOPID controller is stable. Furthermore, the poles of the controller are also evaluated to determine their exact location in the s-plane. The poles of FOPID controller are:

$$\begin{aligned} &POLES_{FOPID} \\ &= -1114.360323 - 306.340269 - 263.297603 \\ &\quad - 91.160771 - 71.621132 - 26.402041 \\ &\quad - 20.240251 - 7.491060 - 5.778317 \\ &\quad - 2.103099 - 1.678388 - 0.602689 \\ &\quad - 0.468771 - 0.174504 - 0.132769 \\ &\quad - 0.049007 - 0.038295 - 0.014017 \\ &\quad - 0.010807 - 0.003995 - 0.003095 \\ &\quad - 0.001132 - 886.486175 - 118.561112i \\ &\quad - 886.486175 + 118.561112i \end{aligned}$$

All the yielded poles for both the FOPID controller and the Maglev system have a negative real value. Hence, it is confirmed that poles exist in the left-half of s plane and the designed FOPID controller and Maglev system both are stable.

IV. SIMULATED RESULTS

There are no analytic solutions for fractional-order differential equations. Various numerical and approximation methods have been proposed in the literature to solve these equations. Ziegler Nichols method and Ant Colony Optimization (ACO) algorithm are the two methods used for tuning the parameters of the controller.

FOPID has been tuned initially with the Ziegler Nicholas method using two sets of rules. These rules for tuning FOPID assumed that the plant has a unit step response with an S-shape, as shown in Figure 10.

where T is the time constant and L is apparent delay, resulting from a pole. Any general plant with this response can be represented using (16):

$$G(s) = \frac{K}{1 + sT} e^{-Ls} \tag{16}$$

The two rules of Ziegler Nicholas method for tuning FOPID are defined as:

1) First rule: First set of rules can be described using (17)

$$\begin{aligned} P = &-0.0048 + 0.4982T - 0.0720T^2 \\ &- 0.0348TL + 0.2664L + 0.0232L^2 \end{aligned} \tag{17}$$

TABLE 4. Routh table FOPID controller.

s^n	a^n	a^{n-2}	a^{n-4}	a^{n-6}	a^{n-8}	a^{n-10}	a^{n-12}	a^{n-14}	a^{n-16}	a^{n-18}	a^{n-20}	a^{n-22}	a^{n-24}
s^{24}	0	0	0	0	0.0012	0.1792	2.2060	2.2020	0.1775	0.0011	0	0	0
s^{23}	0	0	0	0	0.0200	0.8616	3.0220	0.8576	0.0196	0	0	0	0
s^{22}	0	0	0	0.0012	0.1790	2.2052	2.2018	0.1775	0.0011	0	0	0	0
s^{21}	0	0	0	0.0198	0.8597	3.0201	0.8574	0.0196	0	0	0	0	0
s^{20}	0	0	0.001	0.1776	2.2003	2.2004	0.1775	0.011	0	0	0	0	0
s^{19}	0	0	0.0193	0.8523	3.0138	0.8569	0.0196	0	0	0	0	0	0
s^{18}	0	0.0010	0.1733	2.1851	2.1961	0.1774	0.0011	0	0	0	0	0	0
s^{17}	0	0.0177	0.8334	2.9937	0.8553	0.0196	0	0	0	0	0	0	0
s^{16}	0.0007	0.1592	2.1344	2.1816	0.1771	0.0011	0	0	0	0	0	0	0
s^{15}	0.0127	0.7658	2.9246	0.8497	0.0195	0	0	0	0	0	0	0	0
s^{14}	0.1138	1.9613	2.1313	0.1759	0.0011	0	0	0	0	0	0	0	0
s^{13}	0.5477	2.6876	0.8301	0.0194	0	0	0	0	0	0	0	0	0
s^{12}	104027	1.9587	0.1719	0.0011	0	0	0	0	0	0	0	0	0
s^{11}	1.9228	0.7630	0.0190	0	0	0	0	0	0	0	0	0	0
s^{10}	1.4021	0.1580	0.0011	0	0	0	0	0	0	0	0	0	0
s^{9}	0.5463	0.01175	0	0	0	0	0	0	0	0	0	0	0
s^{8}	0.1132	0.0010	0.0011	0	0	0	0	0	0	0	0	0	0
s^{7}	0.0125	0	0	0	0	0	0	0	0	0	0	0	0
s^{6}	0.0007	0	0	0	0	0	0	0	0	0	0	0	0
s^{5}	0	0	0	0	0	0	0	0	0	0	0	0	0
s^{4}	0	0	0	0	0	0	0	0	0	0	0	0	0
s^{3}	0	0	0	0	0	0	0	0	0	0	0	0	0
s^{2}	0	0	0	0	0	0	0	0	0	0	0	0	0
s^{1}	0	0	0	0	0	0	0	0	0	0	0	0	0
s^{0}	0	0	0	0	0	0	0	0	0	0	0	0	0

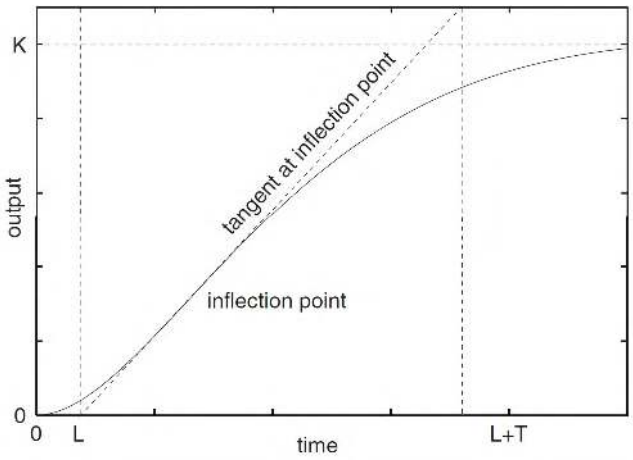

FIGURE 10. Ziegler Nicholas unit step response (S-shaped) [96].

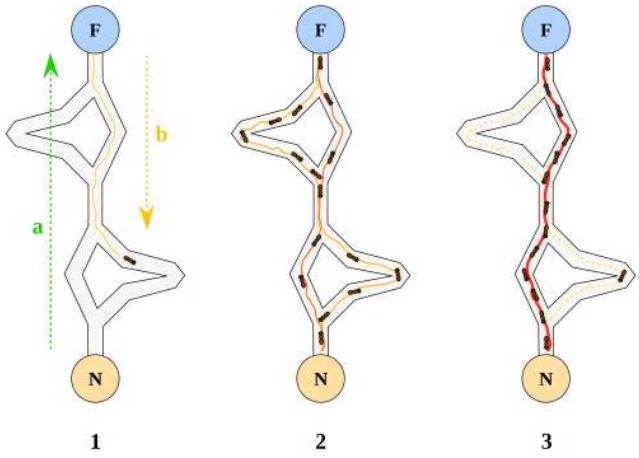

FIGURE 11. Ant colony optimization algorithm process [99].

The boundary values for the first set of rules are: $0.099 < T < 51$ and $L < 2.1$

2) Second rule: The second set of rules are found in the same way using (17) with the following boundary values: $0.099 < T < 50.01$ and $L < 0.51$

A. ANT COLONY OPTIMIZATION (ACO)

Ant Colony Optimization algorithm is best suited for solving various optimization problems. Cooperation between a colony of ants is the key to finding the optimum solution [97]. The nature-inspired ant colony algorithm is based on the natural behavior of the ants. This algorithm is robust, adaptive and can be applied to various problems [98]. The main characteristics of artificial ants can be classified as:

- Colonies of artificial ants exist for cooperation between individuals
- Communication is performed using an indirect method known as pheromone deposition.
- Shortest path between the starting and destination point is found using a sequence of local moves. A stochastic decision policy is applied to find the best solutions using local information only. Figure 11 shows the mathematical optimization of the ACO algorithm.

Artificial ants have few intelligent qualities that are not present in natural ants, to solve particular optimization problems. The solution to the optimizing problem is determined by each ant on their own. It is only when a colony of ants communicate with each other, the best possible solution is

determined. The communication between ants is done by an indirect method that adds the pheromones to the environment. The shortest path to the destination is determined by an ant when it starts from an initial state and makes it path along the sequence of neighboring states.

The local stochastic search policy controls the movement of ants that is governed by the local environmental information, pheromone trails and the internal states [100]. The location and time for releasing the pheromones in the environment are determined by the ants by using private or public information. The movement quality produced by an ant is directly proportional to the number of pheromones released in most of the applications [101]. Higher the number of pheromones, the quicker the solution is achieved. When an ant finds the solution that is not optimum, it dies or gets deleted from the system. The potentially good solutions are formed by ACO through the pheromone matrix ($\Psi = \Psi_{mn}$). Initial values of Ψ are set to be:

$$\Psi_{mn} = \Psi_0 \quad \forall(m, n), \qquad where\ \Psi_0 > 0$$

The selection of node m at node n has the probability $P^Y_{mn}(t)$, as shown in (18). This relation is used by the ants, for complete construction of the solution, in each generation of the algorithm.

$$P^Y_{mn}(t) = \frac{[\Psi_{mn}(t)]^\alpha [\eta_{mn}]^\beta}{\Sigma_{m,n\in T^Y}[\Psi_{mn}(t)]^\alpha [\eta_{mn}]^\beta} \tag{18}$$

If $m, n \in T^Y$, T^Y determines the effectuated path at given time by an ant (Y), constants α and β report the relative influence of heuristic and pheromone values. The heuristic function (η_{mn}) is defined as:

$$\eta_{mn} = \frac{1}{k_n}, n = [p, i^\lambda, d^\mu]$$

Pheromone quantity $\Delta\Psi^Y_{mn}$ at each path is defined by (19).

$$\Delta\Psi^Y_{mn} = \begin{bmatrix} \frac{L^{best}}{L^Y} \\ 0 \end{bmatrix} \tag{19}$$

If $m, n \in T^Y$, L^{best} is the solution found by a set of ants that is best at the current iteration with respect to all previous solutions and L^Y is the objective function's value determined by an ant Y. The increase in pheromones population is avoided by the phenomena known as pheromone evaporation, whereupon yielding a better solution, all previous pheromones are deleted from the system. The evaporation rate of pheromones is described by (20)

$$\Psi_{mn}(t) = p\Psi_{mn}(t-1) + \Sigma^{NY}_{Y=1}\Delta\Psi^Y_{mn}(t) \tag{20}$$

where p is the evaporation rate with boundary values of $0 < p \leqslant 1$ and NY is the number of ants. The parameters of ACO algorithm that are used for tuning the parameters of FOPID controller are: ants=300, population=100, path=50, fitness Function = ISE, iterations=300.

The ACO algorithm is implemented on FOPID controller using the following six steps:

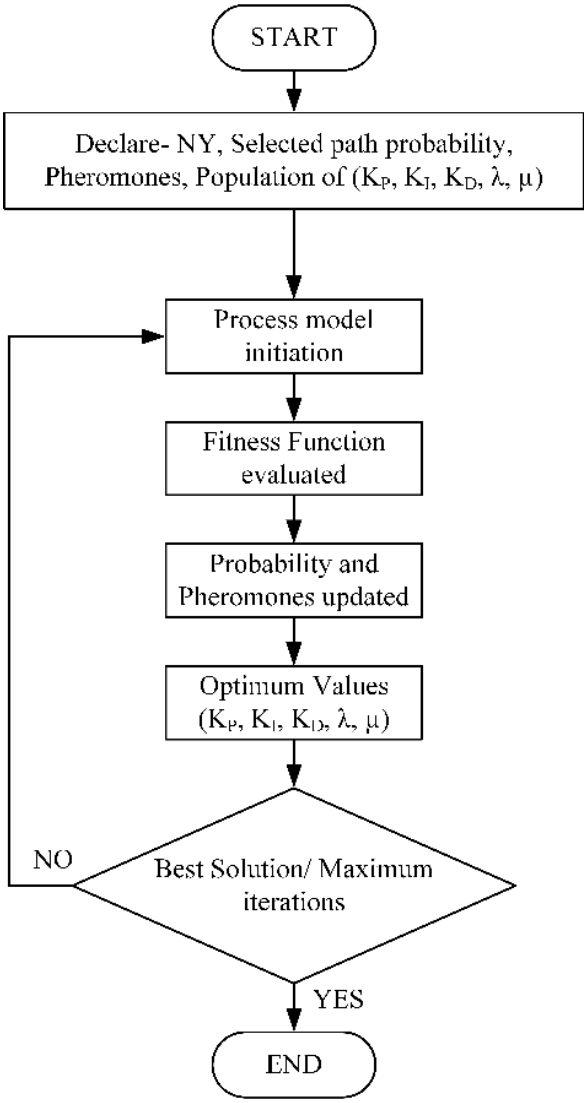

FIGURE 12. Flow chart of ACO algorithm for FOPID controller.

1) Heuristic value, pheromone trail and probable solutions for FOPID parameter ($K_P, K_I, K_D, \lambda, \mu$) are initialized.
2) Y^{th} ant is placed on the node and heuristic value computed is linked with the objective to minimize the error.
3) The population of pheromones is controlled by using (20) and bad choices are allowed to be deleted.
4) The obtained solutions are evaluated in accordance with the objective.
5) The optimum value for the optimized parameters is displayed.
6) Pheromones are updated globally in accordance with the results obtained in step 5. The process is repeated and initiated again from step 2 until the best result or maximum iterations are reached. The flow chart for the whole process of the ACO algorithm for the FOPID controller is shown in Figure 12.

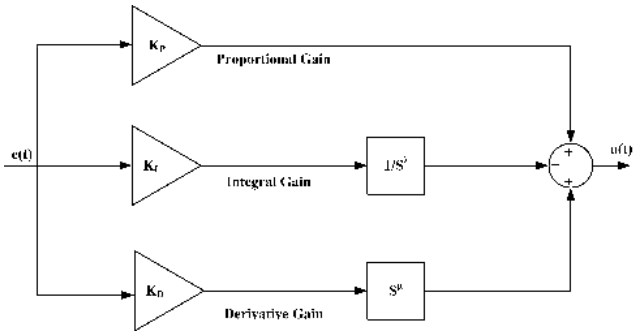

FIGURE 13. FOPID controller block diagram.

V. FOPID CONTROLLER DESIGN

FOPID controller is an implementation of fractional calculus. The conventional IOPID controller is expanded from point to plane and generalized by the fractional order PID controller. The flexibility to controller design is enhanced due to this expansion and a very small control effort is required to accurately control the real life processes. FOPID controllers in closed-loop responses show better results than the conventional IOPID controller because of two new parameters that can be tuned [102]. These two new tuning parameters are the powers of integral and derivative that are non-integer numbers [103]. The five parameters of FOPID controller cause the system to be more robust and flexible and less sensitive to any disturbances that may occur in a controlled plant. The realization of FOPID controller is performed using Oustaloup's approximation method. The control parameters of FOPID and IOPID controller have been optimized by ant colony optimization and artificial bee colony algorithm for comparative analysis.

FOPID has small settling time and low percentage overshoot for slow process plants due to its simplicity of design [104]. It is an extended version of the conventional IOPID controller. Although, it is less sensitive to a controlled system that has varying parameters and it can fall into iso-damping quite easily [105]. Conventional IOPID controllers are also special cases of FOPID controller with $\lambda = 1$ and $\mu = 1$. Various versions of conventional IOPID controller can be described according to the values of λ and μ:

- $\lambda = 0$ and $\mu = 0$ (P controller)
- $\lambda = 1$ and $\mu = 1$ (PID controller)
- $\lambda = 1$ and $\mu = 0$ (PI controller)
- $\lambda = 0$ and $\mu = 1$ (PD controller)

The operations on I and D are normally of fractional order and their range is considered between 0 and 2. Therefore, these two new parameters (λ and μ) are also tuned along with K_P, K_I and K_D. Hence, it requires optimization of all five parameters in five dimensional hyperspace. The general block diagram of the FOPID controller being used in this research is shown in Figure 13.

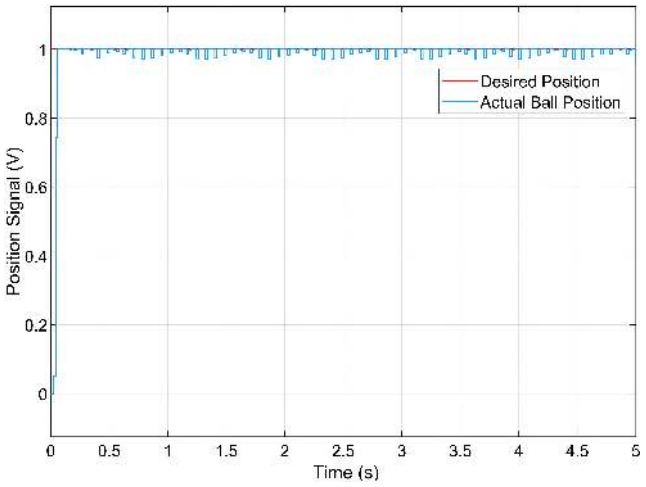

FIGURE 14. Levitating object position signal vs time (Case 1-FOPID).

VI. RESULTS AND DISCUSSIONS

A. CASE 1 (ZIEGLER NICHOLAS METHOD (FOPID))

The system is observed for 5 seconds using tuning parameter values found by Ziegler Nicholas for the FOPID controller and results are shown in Figure 14. These results have used the following values of tuning parameters:

$$K_P = 15.1238 \quad K_I = 19.9856 \; K_D = 8.2105$$
$$\mu = 0.5158 \quad \lambda = 0.4982$$

The yielded results indicate that peak time and rise time are both quite low. Although there are oscillations throughout the simulation and steady-state with zero error is not reached. These results are further improved by using the values of the tuning parameters obtained from the ACO algorithm.

B. CASE 2 (ANT COLONY OPTIMIZATION (FOPID))

The following values of all five parameters have been achieved by using the ACO algorithm and the yielded results are shown in Figure 15.

$$K_P = 15.5223$$
$$K_I = 19.2563$$
$$K_D = 8.3856$$
$$\mu = 0.8554$$
$$\lambda = 0.9189$$

It can be observed that the settling time is reduced to 0.1997 seconds and rise time along with peak time are 0.1587 and 0.2200 seconds, respectively. There are almost no oscillations at all left in the output results and the zero-steady state error is achieved.

The voltage signal fed at the input of the electromagnetic coil is varied to adjust the position of the levitating object. Saturation of coil represents the input voltage signal that comes from the FOPID controller and the magnetic levitation plant model represents the feedback signal that shows the position of the levitating object. The output results of both these signals are shown in Figure 16.

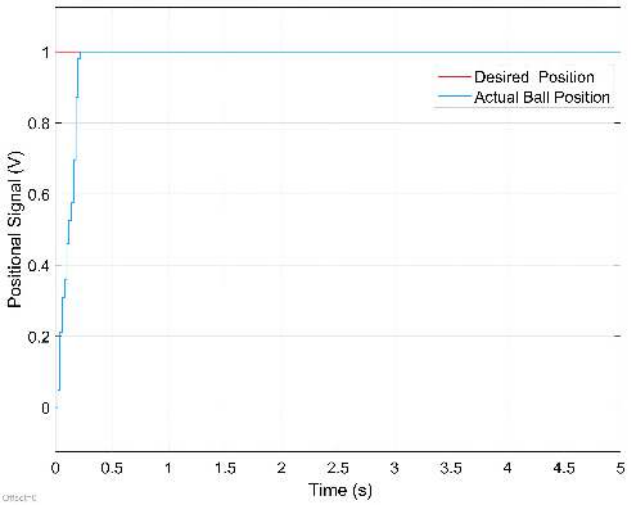

FIGURE 15. Levitating object position signal vs time (Case 2-FOPID).

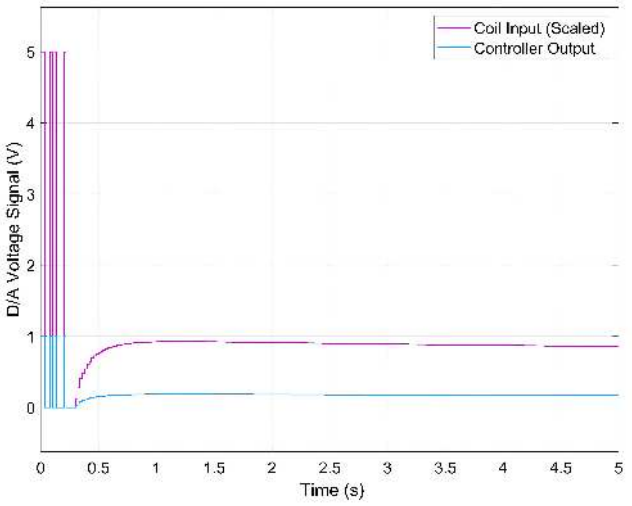

FIGURE 17. Controller output and Electromagnetic coil input signal vs time (Case 2-FOPID).

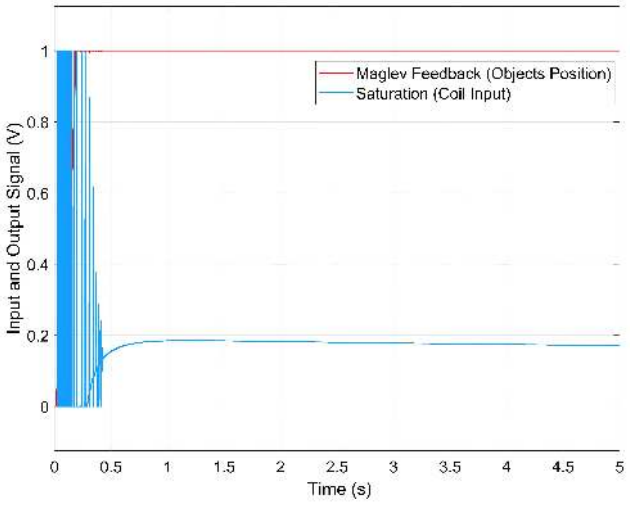

FIGURE 16. Saturation coil and Feedback voltage signal vs time (Case 2-FOPID).

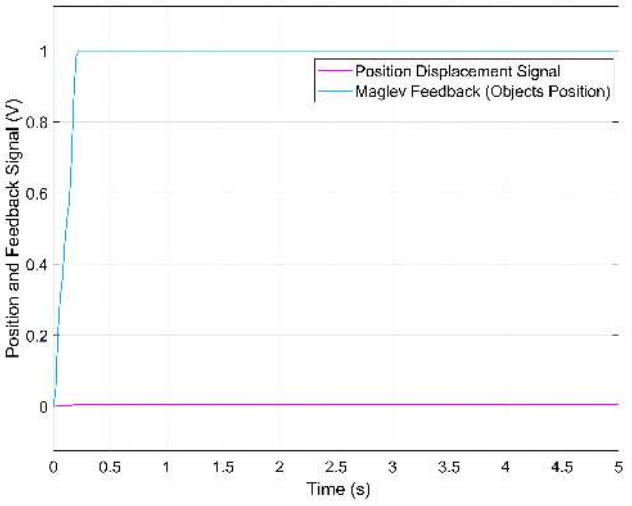

FIGURE 18. Displaced position and feedback (controller input) signal vs time (Case 2-FOPID).

It can be noted that variations in the controller output signal are quite abrupt for a very small period and then a steady-state is achieved. It indicates that the efficiency of the FOPID controller using the ACO algorithm has increased by a significant amount than that of FOPID with the Ziegler Nicholas method. Figure 17 shows the controller output signal that is mapped to the desired range before it is fed to the coil.

The position of the levitating object or the output signal of analog/digital converter is sent as feedback signal to the controller. Figure 18 shows the results of position variations (position) and the generated signal (AD converter and position sensor) that is sent as feedback to the controller.

The velocity signal and position of the levitating object is adjusted with respect to each other to reach a steady-state value. It can be observed in Figure 19 that large variations in the velocity occur with negligible variations in the position for optimum results.

This velocity signal (V) is multiplied with the negative damping gain to reduce the input signal by the required amount. The steady velocity signal keeps the object in a steady-state and its motion in all directions is canceled out. However, any disturbance at the object's position causes the velocity signal to reduce the damping in accordance with the direction of motion.

C. IOPID CONTROLLER (ZIEGLER NICHOLAS Method)

Similarly, the system is observed for 5 seconds using tuning parameter values found by Ziegler Nicholas for the IOPID controller and results are shown in Figure 20. These results have used the following values of tuning parameters:

$$K_P = 0.8985$$
$$K_I = 2.1035$$
$$K_D = 0.0012$$

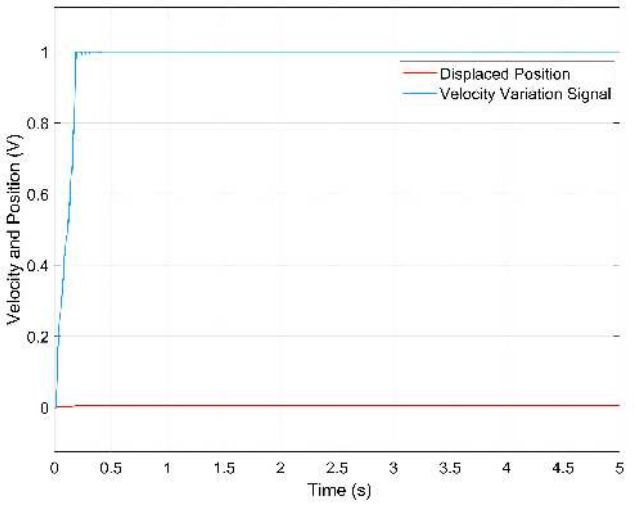

FIGURE 19. Displaced position and damping velocity signal of the levitating object vs time (Case 2-FOPID).

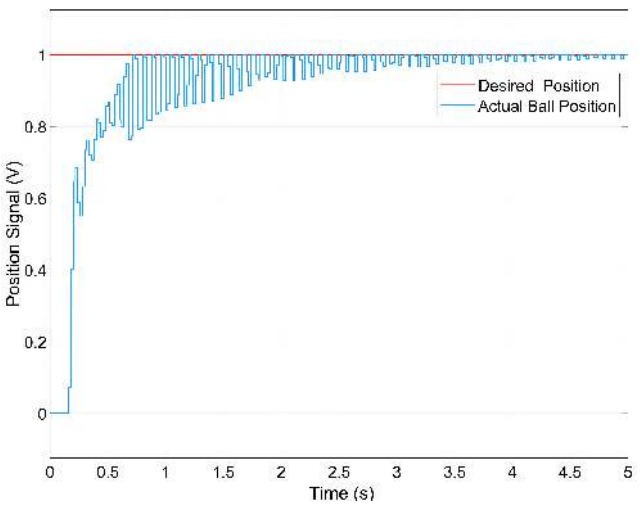

FIGURE 21. Levitating object position signal vs time (IOPID-ACO).

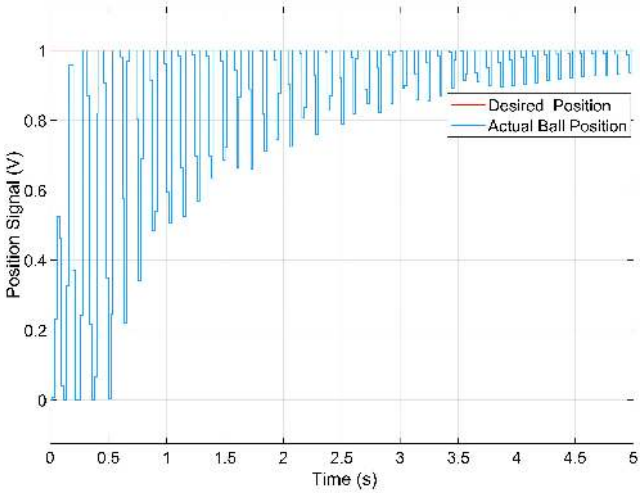

FIGURE 20. Levitating object position signal vs time (IOPID-ZN).

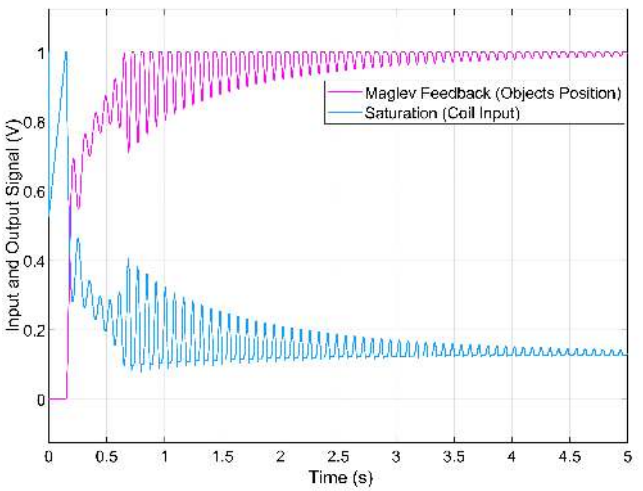

FIGURE 22. Saturation coil and feedback voltage signal vs time (IOPID-ACO).

It can be observed that number of oscillations is quite high and steady state is not reached. Settling time is quite high and overall evaluation is far away from the desired response. These results for the IOPID controller are further improved by using the values of the tuning parameters obtained from the ACO algorithm.

D. IOPID CONTROLLER (Ant COLONY OPTIMIZATION)

The system is observed again for 5 seconds with the following values of tunning parameters that are obtained from the ACO algorithm for IOPID controller:

$$K_P = 0.5245$$
$$K_I = 3.2587$$
$$K_D = 0.0121$$

The position of the object and its oscillations about the mean position are shown in Figure 21.

It can be observed that initially there are transients and the settling time using the IOPID controller is reached at 3.7230 seconds. It can be noted that the oscillations using the IOPID controller have a significant effect on the system as compared to the FOPID controller. As the position of the levitating object is further from the desired position, more force of electromagnetic attraction from the coil is required and hence signal with higher amplitude is fed into the coil. In accordance with the position, the voltage signal is fed throughout until the stability is reached. This can be observed in Figure 22.

The feedback signal is received by the IOPID controller and adjusted through an optimizing algorithm (ACO) before it is fed back to the inductive coil for the next repetitive cycle until the steady-state is achieved. The input signal to the coil is mapped from 0-1 to 0-5 through the digital/analog converter.

TABLE 5. Evaluated parameters analysis of IOPID and FOPID controller with ZN and ACO algorithm.

Controller	Rise Time (s)	Peak Time (s)	Settling Time (s)	Steady State Error (-)	K_p	K_I	K_D	μ	λ
IOPID-ZN	0.1299	0.2800	4.9739	0	0.8985	2.1035	0.0012	1	1
IOPID-ACO	0.4062	0.7200	3.7230	0.0031	0.5245	3.2587	0.0121	1	1
FOPID-ZN (Case-1)	0.0307	0.0600	68.4204	0.0279	15.1238	19.9850	8.2105	0.5158	0.4982
FOPID-ACO (Case-2)	0.1587	0.2200	0.1997	0	15.5223	19.2563	8.3856	0.8554	0.9189

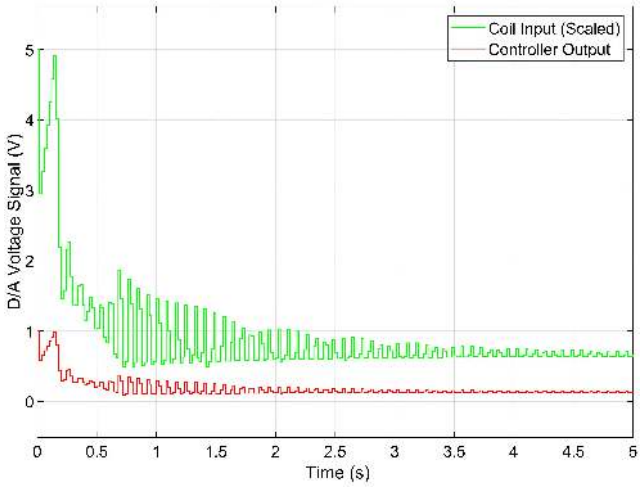

FIGURE 23. Controller output signal and electromagnetic coil input signal vs time (IOPID-ACO).

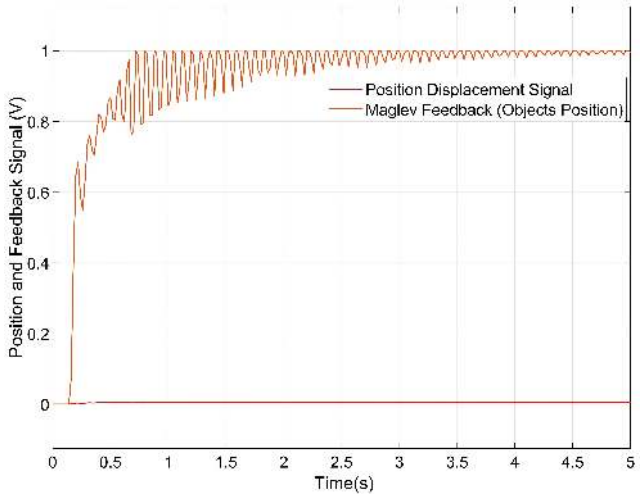

FIGURE 24. Displaced position and feedback (controller input) signal vs time (IOPID-ACO).

Figure 23 shows the input signal and the mapped signal that is given to the coil.

It can be seen that as the oscillations decrease and the levitating object reaches the steady-state about its mean position, the input signal to the coil reaches a steady value and the digital output signal from the controller is almost steady. The input coil signal is not at zero level due to the fact that gravity is pulling the object and electromagnetic force of attraction must exist to counteract its effect. Variations in the position

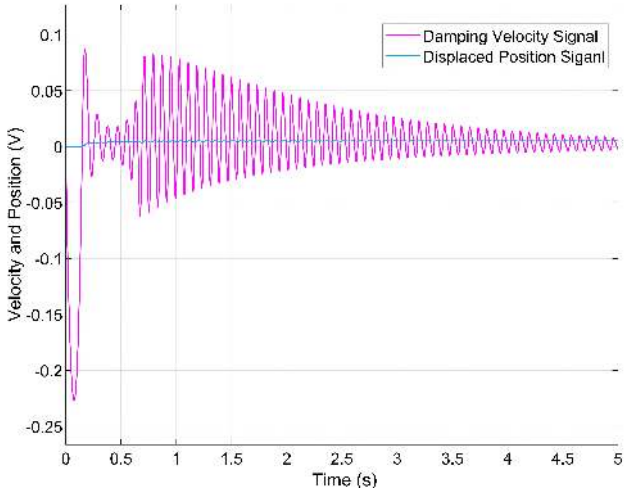

FIGURE 25. Displaced position and damping velocity signal of the levitating object vs time (IOPID-ACO).

TABLE 6. Efficiency analysis of both controllers with ZN and ACO algorithm.

Controller	Rise Time (%)	Peak Time (%)	Settling Time (%)
IOPID-ZN	100	100	100
IOPID-ACO	-212.7	-157.1	25.2
FOPID-ZN (Case-1)	76.37	78.6	-1275.5
FOPID-ACO (Case-2)	-22.2	21.43	95.99

and the output signal of analog/digital converter are sent as feedback to the controller, as shown in Figure 24.

Velocity and position of the levitating object are adjusted to reach a steady-state value. The transients removed through the IOPID controller are shown in Figure 25. It can be observed that variation in the speed of the levitating object is quite large as compared to the FOPID controller.

VII. COMPARATIVE ANALYSIS BETWEEN IOPID AND FOPID

Considering the efficiency of IOPID-ZN to be 100 % as a reference. Table 5 shows the comparative analysis of all evaluated parameters and Table 6 indicates the increase (positive sign) and decrease (negative sign) in efficiency of the magnetic levitation system in each parameter using the IOPID and FOPID controller with ZN and ACO algorithm. It can be noted that FOPID(Case-2) using the ACO algorithm has resulted in the most efficient settling time.

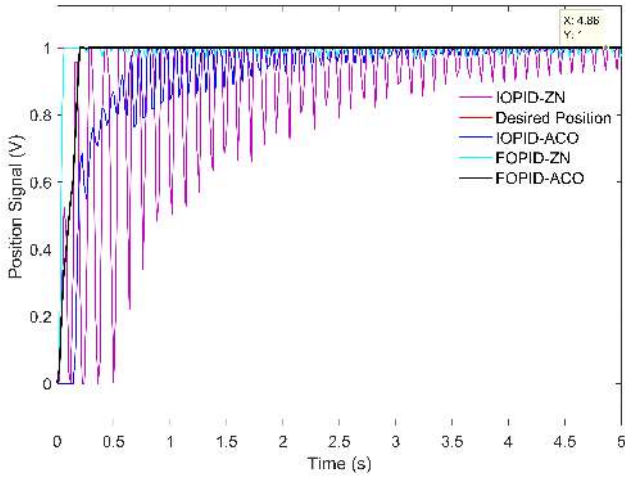

FIGURE 26. Comparative analysis of IOPID and FOPID controller using ACO algorithm and ZN method.

It can be observed in Figure 26 that FOPID-ZN has the least rise time and the longest settling time. FOPID-ACO can be observed to have no oscillations at all after it reaches the desired value with the least settling time. IOPID-ZN produced the most oscillations and a long settling time before reaching a steady state. IOPID-ACO has no oscillations but the settling time is quite long as compared to FOPID-ACO.

VIII. CONCLUSIONS AND FUTURE WORK

The aim of this research is to reduce the settling time of the levitating object to reduce its oscillations. Other parameters, e.g. Rise time, Peak time, Time constant, etc., can also achieve higher accuracy if the research focus is placed on them. The goal of this research has been achieved as the evaluated parameters of Case-2 (FOPID-ACO) show brilliant results and the transients are observed to be negligible and steady-state is reach at a very early stage. The efficiency of settling time has increased by 95.99% in comparison to the traditional IOPID-ZN controller. Even though other evaluated parameters of Case-2 (FOPID-ACO) have not been considered as the main focus, still the efficiency of peak time has increased 21.43 %. Case-1 (FOPID-ZN) of the FOPID controller indicates higher efficiency of rise time and peak time (76.37 and %, 78.6 %), while the settling time is decreased in efficiency by −1275.5 % in comparison to the traditional IOPID-ZN controller.

The ACO algorithm and the Ziegler Nicholas method have been used to adjust the tuning parameters of the controller. ACO algorithm has increased the efficiency and stability of the system as compared to the Ziegler Nicholas method. The performance of FOPID controller with constraints has not been tested yet. In the next phase of research, the Maglev system with constraints, uncertainties and external disturbances will be analyzed and the parameters of the FOPID controller will be improved, to set their values in accordance with any disturbances or constraints at the levitating object, using nature-inspired intelligent optimizing algorithms.

REFERENCES

[1] I. Ahmad and J. Ma, "Nonlinear model & controller design for magnetic levitation system," in *Proc. Recent Adv. Signal Process., Robot. Automat. (ISPRA)*, 2010, pp. 324–328.
[2] E. Anene and G. K. Venayagamoorthy, "PSO tuned flatness based control of a magnetic levitation system," in *Proc. IEEE Ind. Appl. Soc. Annu. Meeting*, Oct. 2010, pp. 1–5.
[3] H. Yaghoubi, "The most important maglev applications," *J. Eng.*, vol. 2013, Mar. 2013, Art. no. 537986, doi: 10.1155/2013/537986.
[4] X. Wei and L. Guo, "Composite disturbance observer based control and H_∞ control for complex continuous models," *Int. J. Robust Nonlinear*, vol. 20, no. 1, pp. 106–118, Jan. 2010, doi: 10.1002/rnc.1425.
[5] F.-J. Lin, L.-T. Teng, and P.-H. Shieh, "Intelligent sliding-mode control using RBFN for magnetic levitation system," *IEEE Trans. Ind. Electron.*, vol. 54, no. 3, pp. 1752–1762, Jun. 2007, doi: 10.1109/TIE.2007.894710.
[6] D. Sain, S. K. Swain, and S. K. Mishra, "TID and I-TD controller design for magnetic levitation system using genetic algorithm," *Perspect. Sci.*, vol. 8, pp. 370–373, Sep. 2016, doi: 10.1016/j.pisc.2016.04.078.
[7] F.-J. Lin, H.-J. Shieh, L.-T. Teng, and P.-H. Shieh, "Hybrid controller with recurrent neural network for magnetic levitation system," *IEEE Trans. Magn.*, vol. 41, no. 7, pp. 2260–2269, Jul. 2005, doi: 10.1109/TMAG.2005.848320.
[8] J. S. Saini, M. Gopal, and A. P. Mittal, "Evolving optimal fuzzy logic controllers by genetic algorithms," *IETE J. Res.*, vol. 50, no. 3, pp. 179–190, May 2004, doi: 10.1080/03772063.2004.11665504.
[9] V. Kachitvichyanukul, "Comparison of three evolutionary algorithms: GA, PSO, and DE," *Ind. Eng. Manage. Syst.*, vol. 11, no. 3, pp. 215–223, Sep. 2012, doi: 10.7232/iems.2012.11.3.215.
[10] M. Milovanovic, D. Antic, S. S. Nikolic, S. Peric, M. Milojkovic, and M. Spasic, "Neural network based on orthogonal polynomials applied in magnetic levitation system control," *Elektronika ir Elektrotechnika*, vol. 23, no. 3, pp. 24–29, Jun. 2017, doi: 10.5755/j01.eie.23.3.13167.
[11] C.-A. Bojan-Dragos, A.-I. Stinean, R.-E. Precup, S. Preitl, and E. M. Petriu, "Model predictive control solution for magnetic levitation systems," in *Proc. 20th Int. Conf. Methods Models Autom. Robot. (MMAR)*, Aug. 2015, pp. 139–144.
[12] S. Sgaverdea, C.-A. Bojan-Dragos, R.-E. Precup, S. Preitl, and A.-I. Stinean, "Model predictive controllers for magnetic levitation systems," in *Proc. IEEE 10th Jubilee Int. Symp. Appl. Comput. Intell. Informat.*, May 2015, pp. 171–176.
[13] D. Antic, M. Milovanovic, S. Nikolic, M. Milojkovic, and S. Peric, "Simulation model of magnetic levitation based on NARX neural networks," *Int. J. Intell. Syst. Appl.*, vol. 5, no. 5, pp. 25–32, Apr. 2013.
[14] I. Sahin and I. Koyuncu, "Design and implementation of neural networks neurons with RadBas, LogSig, and TanSig activation functions on FPGA," *Electron. Electr. Eng.*, vol. 120, no. 4, Apr. 2012, doi: 10.5755/j01.eee.120.4.1452.
[15] M. Lairi and G. Bloch, "A neural network with minimal structure for maglev system modeling and control," in *Proc. IEEE Int. Symp. Intell. Control Intell. Syst. Semiotics*, Sep. 1999, pp. 40–45.
[16] W. Zuo, Y. Zhu, and L. Cai, "Fourier-neural-network-based learning control for a class of nonlinear systems with flexible components," *IEEE Trans. Neural Netw.*, vol. 20, no. 1, pp. 139–151, Jan. 2009.
[17] M. T. Milojkovic, D. S. Antic, S. S. Nikolic, Z. D. Jovanović, and S. L. Peric, "On a new class of quasi-orthogonal filters," *Int. J. Electron.*, vol. 100, no. 10, pp. 1361–1372, Oct. 2013, doi: 10.1080/00207217.2012.743087.
[18] M. Saberi, H. Altafi, and S. M. Alizadeh, "Control of the magnetic suspension system with a three-degree-of-freedom using RBF neural network controller," *Int. J. Comput. Electr. Eng.*, vol. 4, no. 2, pp. 121–126, 2012, doi: 10.7763/IJCEE.2012.V4.462.
[19] P. S. Shiakolas, S. R. VanSchenck, D. Piyabongkarn, and I. Frangeskou, "Magnetic levitation hardware-in-the-loop and MATLAB-based experiments for reinforcement of neural network control concepts," *IEEE Trans. Educ.*, vol. 47, no. 1, pp. 33–41, Feb. 2004, doi: 10.1109/TE.2003.817616.
[20] Y. Qin, H. Peng, F. Zhou, X. Zeng, and J. Wu, "Nonlinear modeling and control approach to magnetic levitation ball system using functional weight RBF network-based state-dependent ARX model," *J. Franklin Inst.*, vol. 352, no. 10, pp. 4309–4338, Oct. 2015, doi: 10.1016/j.jfranklin.2015.06.014.
[21] B. Danković, S. Nikolić, M. Milojković, and Z. Jovanović, "A class of almost orthogonal filters," *J. Circuits, Syst. Comput.*, vol. 18, no. 5, pp. 923–931, Aug. 2009, doi: 10.1142/S0218126609005447.

[22] M. Milojković, S. Nikolić, B. Danković, D. Antić, and Z. Jovanović, "Modelling of dynamical systems based on almost orthogonal polynomials," *Math. Comput. Model. Dyn. Syst.*, vol. 16, no. 2, pp. 133–144, May 2010, doi: 10.1080/13873951003740082.

[23] D. Antić, B. Danković, S. Nikolić, M. Milojković, and Z. Jovanović, "Approximation based on orthogonal and almost orthogonal functions," *J. Franklin Inst.*, vol. 349, no. 1, pp. 323–336, Feb. 2012, doi: 10.1016/j.jfranklin.2011.11.006.

[24] S. S. Nikolić, D. S. Antic, M. T. Milojković, M. B. Milovanović, S. L. Peric, and D. B. Mitic, "Application of neural networks with orthogonal activation functions in control of dynamical systems," *Int. J. Electron.*, vol. 103, no. 4, pp. 667–685, Apr. 2016, doi: 10.1080/00207217.2015.1036811.

[25] S. S. Nikolić, D. S. Antic, S. L. Peric, N. B. Dankovic, and M. T. Milojković, "Design of generalised orthogonal filters: Application to the modelling of dynamical systems," *Int. J. Electron.*, vol. 103, no. 2, pp. 269–280, Feb. 2016, doi: 10.1080/00207217.2015.1036367.

[26] B. Ataslar-Ayyildiz and O. Karahan, "Trajectory tracking for the magnetic ball levitation system via fuzzy PID control based on CS algorithm," in *Proc. IEEE Int. Symp. Innov. Intell. Syst. Appl. (INISTA)*, Jul. 2019, pp. 1–6, doi: 10.1109/INISTA.2019.8778271.

[27] I. Pan and S. Das, "Frequency domain design of fractional order PID controller for AVR system using chaotic multi-objective optimization," *Int. J. Electr. Power Energy Syst.*, vol. 51, pp. 106–118, Oct. 2013, doi: 10.1016/j.ijepes.2013.02.021.

[28] I. Ahmad, M. Shahzad, and P. Palensky, "Optimal PID control of magnetic levitation system using genetic algorithm," in *Proc. IEEE Int. Energy Conf. (ENERGYCON)*, May 2014, pp. 1429–1433, doi: 10.1109/ENERGYCON.2014.6850610.

[29] S. Yadav, S. K. Verma, and S. K. Nagar, "Optimized PID controller for magnetic levitation system," *IFAC-PapersOnLine*, vol. 49, no. 1, pp. 778–782, 2016, doi: 10.1016/j.ifacol.2016.03.151.

[30] E. Vinodh Kumar and J. Jerome, "LQR based optimal tuning of PID controller for trajectory tracking of magnetic levitation system," *Procedia Eng.*, vol. 64, pp. 254–264, Jan. 2013, doi: 10.1016/j.proeng.2013.09.097.

[31] M. H. A. Yaseen and H. J. Abd, "Modeling and control for a magnetic levitation system based on SIMLAB platform in real time," *Results Phys.*, vol. 8, pp. 153–159, Mar. 2018, doi: 10.1016/j.rinp.2017.11.026.

[32] J. de Jesús Rubio, L. Zhang, E. Lughofer, P. Cruz, A. Alsaedi, and T. Hayat, "Modeling and control with neural networks for a magnetic levitation system," *Neurocomputing*, vol. 227, pp. 113–121, Mar. 2017, doi: 10.1016/j.neucom.2016.09.101.

[33] M. Strumik, R. Wawrzaszek, M. Banaszkiewicz, K. Seweryn, M. Sidz, E. Onillon, and L. Rossini, "Analytical model of eddy currents in a reaction sphere actuator," *IEEE Trans. Magn.*, vol. 50, no. 6, pp. 1–7, Jun. 2014, doi: 10.1109/TMAG.2014.2298215.

[34] M. T. Thompson, "Electrodynamic magnetic suspension-models, scaling laws, and experimental results," *IEEE Trans. Educ.*, vol. 43, no. 3, pp. 336–342, Aug. 2000, doi: 10.1109/13.865211.

[35] W. Yu, P. C. Francisco, and X. Li, "Two-stage neural sliding-mode control of magnetic levitation in minimal invasive surgery," *Neural Comput. Appl.*, vol. 20, no. 8, pp. 1141–1147, Nov. 2011, doi: 10.1007/s00521-010-0477-2.

[36] A. Goel and A. Swarup, "A novel high-order sliding mode control of magnetic levitation system," in *Proc. IEEE 59th Int. Midwest Symp. Circuits Syst. (MWSCAS)*, Oct. 2016, pp. 1–4, doi: 10.1109/MWSCAS.2016.7870019.

[37] A. Swarup, "High order super twisting sliding mode control of robotic manipulator," *ICIC Exp. Lett. Int. J. Res. Surv.*, vol. 6, no. 11, pp. 3095–3101, 2015.

[38] N. F. Al-Muthairi and M. Zribi, "Sliding mode control of a magnetic levitation system," *Math. Problems Eng.*, vol. 2004, no. 2, pp. 93–107, 2004, doi: 10.1155/S1024123X04310033.

[39] N. Boonsatit and C. Pukdeboon, "Adaptive fast terminal sliding mode control of magnetic levitation system," *J. Control, Autom. Electr. Syst.*, vol. 27, no. 4, pp. 359–367, Aug. 2016, doi: 10.1007/s40313-016-0246-2.

[40] A. El Hajjaji and M. Ouladsine, "Modeling and nonlinear control of magnetic levitation systems," *IEEE Trans. Ind. Electron.*, vol. 48, no. 4, pp. 831–838, Aug. 2001, doi: 10.1109/41.937416.

[41] W. Barie and J. Chiasson, "Linear and nonlinear state-space controllers for magnetic levitation," *Int. J. Syst. Sci.*, vol. 27, no. 11, pp. 1153–1163, Nov. 1996, doi: 10.1080/00207729608929322.

[42] D. L. Trumper, S. M. Olson, and P. K. Subrahmanyan, "Linearizing control of magnetic suspension systems," *IEEE Trans. Control Syst. Technol.*, vol. 5, no. 4, pp. 427–438, Jul. 1997, doi: 10.1109/87.595924.

[43] J. Xu and Y. Zhou, "A nonlinear control method for the electromagnetic suspension system of the maglev train," *J. Modern Transp.*, vol. 19, no. 3, pp. 176–180, Sep. 2011.

[44] U. Sadek, A. Sarjaš, A. Chowdhury, and R. Svecko, "Improved adaptive fuzzy backstepping control of a magnetic levitation system based on symbiotic organism search," *Appl. Soft Comput.*, vol. 56, pp. 19–33, Jul. 2017, doi: 10.1016/j.asoc.2017.02.032.

[45] A. S. Malik, I. Ahmad, A. U. Rahman, and Y. Islam, "Integral backstepping and synergetic control of magnetic levitation system," *IEEE Access*, vol. 7, pp. 173230–173239, 2019, doi: 10.1109/ACCESS.2019.2952551.

[46] P. Šuster and A. Jadlovska, "Modeling and control design of magnetic levitation system," in *Proc. SAMI*, 2012, pp. 295–299.

[47] O.-S. Kim, S.-H. Lee, and D.-C. Han, "Positioning performance and straightness error compensation of the magnetic levitation stage supported by the linear magnetic bearing," *IEEE Trans. Ind. Electron.*, vol. 50, no. 2, pp. 374–378, Apr. 2003, doi: 10.1109/TIE.2003.809415.

[48] L. Qi, J. Cai, A. Han, J. Wan, C. Mei, and Y. Luo, "A novel nonlinear control technique with its application to magnetic levitated systems," *IEEE Access*, vol. 6, pp. 78659–78665, 2018, doi: 10.1109/ACCESS.2018.2885135.

[49] H.-W. Lee, K.-C. Kim, and J. Lee, "Review of maglev train technologies," *IEEE Trans. Magn.*, vol. 42, no. 7, pp. 1917–1925, Jul. 2006, doi: 10.1109/TMAG.2006.875842.

[50] J. Kaloust, C. Ham, J. Siehling, E. Jongekryg, and Q. Han, "Nonlinear robust control design for levitation and propulsion of a maglev system," *IEE Proc. Control Theory Appl.*, vol. 151, no. 4, pp. 460–464, Jul. 2004, doi: 10.1049/ip-cta:20040547.

[51] B. V. Jayawant, W. R. C. Dawson, L. S. Wickramaratne, J. D. Edwards, and T. C. Yang, "Electromagnetic launch assistance for space vehicles," *IET Sci., Meas. Technol.*, vol. 2, no. 1, pp. 42–52, Jan. 2008, doi: 10.1049/iet-smt:20060145.

[52] R. F. Post and D. D. Ryutov, "The inductrack: A simpler approach to magnetic levitation," *IEEE Trans. Appiled Supercond.*, vol. 10, no. 1, pp. 901–904, Mar. 2000, doi: 10.1109/77.828377.

[53] R.-J. Wai and J.-D. Lee, "Robust levitation control for linear maglev rail system using fuzzy neural network," *IEEE Trans. Control Syst. Technol.*, vol. 17, no. 1, pp. 4–14, Jan. 2009, doi: 10.1109/TCST.2008.908205.

[54] A. H. ElSinawi and S. Emam, "Dual LQG-PID control of a highly nonlinear magnetic levitation system," in *Proc. 4th Int. Conf. Modeling, Simulation Appl. Optim.*, Apr. 2011, pp. 1–4.

[55] M. Klauco, M. Kalúz, and M. Kvasnica, "Real-time implementation of an explicit MPC-based reference governor for control of a magnetic levitation system," *Control Eng. Pract.*, vol. 60, pp. 99–105, Mar. 2017, doi: 10.1016/j.conengprac.2017.01.001.

[56] A. Bemporad, "Reference governor for constrained nonlinear systems," *IEEE Trans. Autom. Control*, vol. 43, no. 3, pp. 415–419, Mar. 1998, doi: 10.1109/9.661611.

[57] F. Borrelli, P. Falcone, J. Pekar, and G. Stewart, "Reference governor for constrained piecewise affine systems," *J. Process Control*, vol. 19, no. 8, pp. 1229–1237, Sep. 2009, doi: 10.1016/j.jprocont.2009.06.001.

[58] E. G. Gilbert and I. Kolmanovsky, "Fast reference governors for systems with state and control constraints and disturbance inputs," *Int. J. Robust Nonlinear Control, IFAC-Affiliated J.*, vol. 9, no. 15, pp. 1117–1141, 1999, doi: 10.1002/(SICI)1099-1239(19991230)9:15<1117::AID-RNC447>3.0.CO;2-I.

[59] M. Kaluz, M. Klauco, and M. Kvasnica, "Real-time implementation of a reference governor on the Arduino microcontroller," in *Proc. 20th Int. Conf. Process Control (PC)*, Jun. 2015, pp. 350–356.

[60] T. Bächle, S. Hentzelt, and K. Graichen, "Nonlinear model predictive control of a magnetic levitation system," *Control Eng. Pract.*, vol. 21, no. 9, pp. 1250–1258, Sep. 2013, doi: 10.1016/j.conengprac.2013.04.009.

[61] M. Maciejowski, *Predictive Control With Constraints*. London, U.K.: Pearson, 2002.

[62] D. Q. Mayne, J. B. Rawlings, C. V. Rao, and P. O. M. Scokaert, "Constrained model predictive control: Stability and optimality," *Automatica*, vol. 36, no. 6, pp. 789–814, 2000, doi: 10.1016/S0005-1098(99)00214-9.

[63] T. Glück, W. Kemmetmüller, C. Tump, and A. Kugi, "A novel robust position estimator for self-sensing magnetic levitation systems based on least squares identification," *Control Eng. Pract.*, vol. 19, no. 2, pp. 146–157, Feb. 2011, doi: 10.1016/j.conengprac.2010.11.003.

[64] A. T. Tran, S. Suzuki, and N. Sakamoto, "Nonlinear optimal control design considering a class of system constraints with validation on a magnetic levitation system," *IEEE Control Syst. Lett.*, vol. 1, no. 2, pp. 418–423, Oct. 2017, doi: 10.1109/LCSYS.2017.2717932.
[65] A. T. Tran and N. Sakamoto, "A general framework for constrained optimal control based on stable manifold method," in *Proc. IEEE 55th Conf. Decis. Control (CDC)*, Dec. 2016, pp. 4886–4893.
[66] N. Sakamoto and A. J. van der Schaft, "Analytical approximation methods for the stabilizing solution of the Hamilton–Jacobi equation," *IEEE Trans. Autom. Control*, vol. 53, no. 10, pp. 2335–2350, Nov. 2008, doi: 10.1109/TAC.2008.2006113.
[67] N. Sakamoto, "Analysis of the Hamilton–Jacobi equation in nonlinear control theory by symplectic geometry," *SIAM J. Control Optim.*, vol. 40, no. 6, pp. 1924–1937, Jan. 2002, doi: 10.1137/S0363012999362803.
[68] L. E. Venghi, G. N. Gonzalez, and F. M. Serra, "Implementation and control of a magnetic levitation system," *IEEE Latin Amer. Trans.*, vol. 14, no. 6, pp. 2651–2656, Jun. 2016, doi: 10.1109/TLA.2016.7555233.
[69] M. Li, P. Zhou, Z. Zhao, and J. Zhang, "Two-degree-of-freedom fractional order-PID controllers design for fractional order processes with dead-time," *ISA Trans.*, vol. 61, pp. 147–154, Mar. 2016, doi: 10.1016/j.isatra.2015.12.007.
[70] M. Araki and H. Taguchi, "Two-degree-of-freedom PID controllers," *Int. J. Control, Automat., Syst.*, vol. 1, no. 4, pp. 401–411, Dec. 2003.
[71] V. Mehra, S. Srivastava, and P. Varshney, "Fractional-order PID controller design for speed control of DC motor," in *Proc. 3rd Int. Conf. Emerg. Trends Eng. Technol. (ICETET)*, Nov. 2010, pp. 422–425.
[72] A. S. Chopade, S. W. Khubalkar, A. S. Junghare, M. V. Aware, and S. Das, "Design and implementation of digital fractional order PID controller using optimal pole-zero approximation method for magnetic levitation system," *IEEE/CAA J. Automatica Sinica*, vol. 5, no. 5, pp. 977–989, Sep. 2018, doi: 10.1109/JAS.2016.7510181.
[73] S. Pandey, P. Dwivedi, and A. S. Junghare, "A novel 2-DOF fractional-order PI^{λ}–D^{μ} controller with inherent anti-windup capability for a magnetic levitation system," *AEU-Int. J. Electron. Commun.*, vol. 79, pp. 158–171, Sep. 2017, doi: 10.1016/j.aeue.2017.05.031.
[74] Y. Zhang, Z. Zheng, J. Zhang, and L. Wang, "Research on fractional order PID controller in magnetic levitation control system," *Int. J. Simul. Syst., Sci. Technol.*, vol. 17, no. 37, pp. 24–31, Nov. 2020.
[75] A. Abbas, S. Z. Hassan, T. Murtaza, A. Mughees, T. Kamal, M. A. Khan, and Q. D. Memon, "Design and control of magnetic levitation system," in *Proc. ICECCE*, Punjab, Pakistan, 2019, pp. 1–5.
[76] P. Shah and S. Agashe, "Review of fractional PID controller," *Mechatronics*, vol. 38, pp. 29–41, Sep. 2016, doi: 10.1016/j.mechatronics.2016.06.005.
[77] L. Majhi, P. Roy, and B. K. Roy, "Design of PID and FOPID controllers tuned by Firefly algorithm for magnetic levitation system," in *Proc. SocProS*, New Dehli, India, 2015, pp. 417–430.
[78] P. Roy, M. Borah, L. Majhi, and N. Singh, "Design and implementation of FOPID controllers by PSO, GSA and PSOGSA for MagLev system," in *Proc. Int. Symp. Adv. Comput. Commun. (ISACC)*, Sep. 2015, pp. 10–15, doi: 10.1109/ISACC.2015.7377307.
[79] M. A. Akram, I. Haider, H.-U.-R. Khalid, and V. Uddin, "Sliding mode control for electromagnetic levitation system based on feedback linearization," in *Proc. Pattern Recognit. Assoc. South Afr. Robot. Mechatronics Int. Conf. (PRASA-RobMech)*, Nov. 2015, pp. 78–82.
[80] A. S. Chopade, L. Jonathan, A. S. Junghare, and M. V. Aware, "Hardware in Loop, real time implementation of Fractional Order PID controller on Magnetic Levitation System," in *Proc. SACI*, 2014, pp. 1–26.
[81] Z. Jing and X. U. Lin, "Fuzzy adaptive PID control in magnetic levitation system," *J. Comput. Appl.*, vol. 29, no. 6, pp. 329–334, Jun. 2009.
[82] J. Zhang, X. Pei, and H. Xing, "Improved RBF neural network control of magnetic levitation [J]," *J. Harbin Univ. Sci. Technol.*, vol. 1, pp. 48–52, 2011.
[83] X. Wang and G. Zhang, "Magnetic levitating bearing control system simulation based on variable universe fuzzy PID algorithm," *Instrum. Technique Sensor*, vol. 12, no. 12, pp. 144–147, 2012.
[84] S. K. Swain, D. Sain, S. K. Mishra, and S. Ghosh, "Real time implementation of fractional order PID controllers for a magnetic levitation plant," *AEU Int. J. Electron. Commun.*, vol. 78, pp. 141–156, Aug. 2017, doi: 10.1016/j.aeue.2017.05.029.
[85] S. Yadav, S. K. Verma, and S. K. Nagar, "Performance enhancement of magnetic levitation system using teaching learning based optimization," *Alexandria Eng. J.*, vol. 57, no. 4, pp. 2427–2433, Dec. 2018, doi: 10.1016/j.aej.2017.08.016.
[86] G. Altintas and Y. Aydin, "Optimization of fractional and integer order PID parameters using big bang big crunch and genetic algorithms for a MAGLEV system," *IFAC-PapersOnLine*, vol. 50, no. 1, pp. 4881–4886, Jul. 2017, doi: 10.1016/j.ifacol.2017.08.978.
[87] B. D. Halilu, E. C. Anene, E. E. Omigzegba, L. Maijama'a, and S. A. Baraza, "Optimization of PID controller gains for identified magnetic levitation plant using bacteria foraging algorithm," *Int. J. Eng. Modern Technol.*, vol. 5, pp. 12–18, Aug. 2019.
[88] R. Song and Z. Chen, "Design of PID controller for maglev system based on an improved PSO with mixed inertia weight," *J. Netw.*, vol. 9, no. 6, p. 1509, Jun. 2014.
[89] B. Nagaraj and N. Murugananth, "A comparative study of PID controller tuning using GA, EP, PSO and ACO," in *Proc. Int. Conf. Commun. Control Comput. Technol. (ICCCCT)*, Oct. 2010, pp. 305–313.
[90] P. Huy, "Beyond the black box: A case study in c to java conversion and product extensibility," Softw. Eng. Inst., Carnegie Mellon Univ., Pittsburgh, PA, USA, Tech. Rep. CMU/SEI-2001-TN-017, 2001.
[91] D. M. Himmelblau and J. B. Riggs, *Basic Principles and Calculations in Chemical Engineering*. Upper Saddle River, NJ, USA: FT Press, 2012.
[92] K. C. Tan and Y. Li, "Grey-box model identification via evolutionary computing," *Control Eng. Pract.*, vol. 10, no. 7, pp. 673–684, Jul. 2002, doi: 10.1016/S0967-0661(02)00031-X.
[93] S. Folea, C. I. Muresan, R. De Keyser, and C. M. Ionescu, "Theoretical analysis and experimental validation of a simplified fractional order controller for a magnetic levitation system," *IEEE Trans. Control Syst. Technol.*, vol. 24, no. 2, pp. 663–756, Jul. 2015, doi: 10.1109/TCST.2015.2446496.
[94] E. Shameli, M. B. Khamesee, and J. P. Huissoon, "Nonlinear controller design for a magnetic levitation device," *Microsyst. Technol.*, vol. 13, nos. 8–10, pp. 831–835, Apr. 2007.
[95] J. M. Araújo and T. L. M. Santos, "Control of a class of second-order linear vibrating systems with time-delay: Smith predictor approach," *Mech. Syst. Signal Process.*, vol. 108, pp. 173–187, Aug. 2018, doi: 10.1016/j.ymssp.2018.02.013.
[96] D. Valério and J. S. Da Costa, "Tuning of fractional PID controllers with Ziegler–Nichols-type rules," *Signal Process.*, vol. 86, no. 10, pp. 2771–2784, Oct. 2006, doi: 10.1016/j.sigpro.2006.02.020.
[97] F. A. G. S. Babu and S. B. T. Chiranjeevi, "Implementation of fractional order PID controller for an AVR system using GA and ACO optimization techniques," *IFAC-PapersOnLine*, vol. 49, no. 1, pp. 456–461, 2016, doi: 10.1016/j.ifacol.2016.03.096.
[98] M. Aabid, A. Elakkary, and N. Sefiani, "PID parameters optimization using ant-colony algorithm for human heart control," in *Proc. ICAC*, 2017, pp. 1–6.
[99] M. D. Toksari, "A hybrid algorithm of ant colony optimization (ACO) and iterated local search (ILS) for estimating electricity domestic consumption: Case of turkey," *Int. J. Electr. Power Energy Syst.*, vol. 78, pp. 776–782, Jun. 2016, doi: 10.1016/j.ijepes.2015.12.032.
[100] G. Wang, "A comparative study of cuckoo algorithm and ant colony algorithm in optimal path problems," in *Proc. MATEC Web Conf.*, vol. 232, 2018, p. 03003.
[101] D. Sandoval, I. Soto, and P. Adasme, "Control of direct current motor using ant colony optimization," in *Proc. Conf. Electr., Electron. Eng., Inf. Commun. Technol. (CHILECON)*, Oct. 2015, pp. 79–82.
[102] D. K. Lal and A. K. Barisal, "Combined load frequency and terminal voltage control of power systems using moth flame optimization algorithm," *J. Electr. Syst. Inf. Technol.*, vol. 6, no. 1, p. 8, Dec. 2019, doi: 10.1186/s43067-019-0010-3.
[103] R. K. Sahu, B. Shaw, and J. R. Nayak, "Fractional-order PID controller optimized by SCA for solar system," in *Proc. AISGSC*, Jan. 2019, pp. 1–10, doi: 10.1007/978-3-030-24051-6_1.
[104] A. Tepljakov, E. Petlenkov, J. Belikov, and E. A. Gonzalez, "Design of retuning fractional PID controllers for a closed-loop magnetic levitation control system," in *Proc. 13th Int. Conf. Control Autom. Robot. Vis. (ICARCV)*, Dec. 2014, pp. 1345–1350.
[105] A. M. A.-H. Shata, R. A. Hamdy, A. S. Abdelkhalik, and I. El-Arabawy, "A fractional order PID control strategy in active magnetic bearing systems," *Alexandria Eng. J.*, vol. 57, no. 4, pp. 3985–3993, Dec. 2018, doi: 10.1016/j.aej.2018.01.020.

ABDULLAH MUGHEES (Member, IEEE) was born in Faisalabad, Punjab, Pakistan, in 1997. He received the B.Sc. degree in electrical engineering from Government College University Faisalabad (GCUF), Punjab, in 2018. He is currently pursuing the M.S. degree in electrical engineering with the FAST National University of Computer and Emerging Sciences.

He is an Expert in robotics, MEMS technology, and control engineering application, and has done numerous research projects for international companies as a Freelancer. He is registered with the Pakistan Engineering Council and is authorized to supervise projects. He has a strong interest in designing innovative applied engineering applications. His research interests include control engineering, robotics, artificial intelligence, applied physics, and electromagnetic theory.

Dr. Mughees has been an Active Student Member of the IEEE since 2014. He has served as the Branch Chair of the IEEE GCUF from 2017 to 2018.

SYED ALI MOHSIN (Member, IEEE) received the B.Sc. degree in electrical engineering from the University of Engineering and Technology (UET) Lahore, Lahore, Pakistan, in 1986, the M.S. degree in electrical engineering from The University of Texas at Austin, Austin, TX, USA, in 1991, and the Ph.D. degree in electrical engineering from UET Lahore, in 2008.

From August 2006 to December 2007, he was a Research Scholar with Purdue University, West Lafayette, IN, USA, where he completed his Ph.D. research. He has served as a Lecturer on the faculties of Kuwait University, as an Assistant Professor with Bahauddin Zakaria University, as an Associate Professor with UET Lahore, and as a Professor with the University of Faisalabad. Since 2015, he has been a Professor with the Department of Electrical Engineering, FAST National University of Computer and Emerging Sciences. His research interests include electromagnetic theory, computational electromagnetics, and their applications in electrical engineering and in biomedical engineering. His research interest includes control engineering.

Dr. Mohsin is a Professional Engineer and a Life Member of the Pakistan Engineering Council (PEC).